Non-Ohmic Variable Range Hopping
in
Lightly Doped Semiconductors

by

Aurora Voje

THESIS
for the degree of
Master of Science

in Condensed Matter Physics

Faculty of Mathematics and Natural Sciences
University of Oslo

June 2009

Det matematisk- naturvitenskapelige fakultet
Universitetet i Oslo

Acknowledgements

The biggest thank you I dedicate to my supervisor Joakim Bergli: In the world of strong long range Coulomb interactions I would be lost without you. Thank you so much for your patience and all the time you spent on widening my horizons, I'll never forget it. Your devotion to the subject has been of a great inspiration.

Next I would like to thank my co-supervisor Yuri Galperin for advice and ideas, for answering all my e-mail requests despite the busy calendar, and for always being helpful and encouraging.

I'd also like to thank Martin Kirkengen for including me in the Coulomb Glass project, for developing the simulation programme, showing me the use of Python and for introducing me to the hopping theory.

I owe Miguel Ortuño and his group a big thank you for the collaboration, for answering my questions and for the wonderful trip to Murcia.

I thank all the members of the AMCS-group for their kindness and for helping me out with all sort of technical problems. A special thank to Karl Eliassen for helping me with most about everything and to Pop for those numerous hours of Matlab-support.

A sincere gratitude goes to Thomas, my family and my friends. Thank you all for the moral support, for helping me through the times of frustration, and for your patience.

Aurora Voje

Oslo, June 2009

Abstract

In this project we have focused on the low temperature electron transport in hopping insulators. At temperatures close to the absolute zero the transport occurs by thermally activated Variable Range Hopping between Anderson localized states. Systems of this kind have been studied for decades and the first models were originally constructed for the lightly doped, compensated semiconductors. In our case the strong, long range Coulomb interactions between the carriers and the dopants are taken into account. The interactions cause a depletion of the density of states near the Fermi level, also known as the Coulomb gap. This strongly influences the system's conductivity.

We have performed numerical Monte Carlo simulations of single electron jumps, and investigated the transport effects when the system is influenced by an electric field. In the linear, Ohmic regime we investigate the Coulomb gap and compare the conductance behaviour to the one predicted by Efros and Shklovskii. In the non-Ohmic case we compare our results to the experimental studies by Aronzon et al. We also observe that the system can be described by two temperatures, a real and an effective one, as the system is heated by the electric field. The effective temperature is extracted from the site occupancy probability distribution which we find is close to the Fermi-Dirac distribution. The results open up for several theoretical questions regarding the relation between the transport, field strength and the effective temperature. A couple of preliminary ideas on how to answer these are introduced.

Contents

Acknowledgements **iii**

Abstract **v**

1 Lightly Doped Semiconductors **1**
1.1 Energy Band Structure. 1
1.2 Doping and compensation. 3
1.2.1 The Hydrogenic Features of Dopants 4
1.3 Localization of Electronic States 8

2 Conductivity in LDS **9**
2.1 Hopping Conduction 11
2.2 Conductivity Through Percolation 14
2.3 Mott's Law and Variable Range Hopping 19
2.3.1 Discussion on the Assumptions in Mott's Law 22
2.4 The Coulomb Gap 23
2.5 The Efros - Shklovskii Law 25
2.6 Non-Ohmic Variable Range Hopping 27

3 The Coulomb Glass Model **31**
3.1 The lattice model 34
3.2 The Dynamic Algorithm 35
3.2.1 The Monte Carlo cycle and the duration of a jump in real time. 39

4 Ohmic Conductivity **43**
4.1 System under influence of an electric field 43
4.2 Electric field strength 43
4.3 Conductivity and lattice size 47
4.4 Confirmation of Efros-Shklovskii law 51
4.4.1 Numerical precision of the p-exponent. 56

5 Non-Ohmic Conductivity **59**
5.1 Effective Temperature in the Non-Ohmic Regime 67
5.1.1 Estimation of the Effective Temperature T_{eff}. 68
5.2 The System Heat Dissipation. 79
5.2.1 Heat emission map 83

6 Discussion **85**

A Miller-Abrahams Hopping Rate **87**

Bibliography **94**

Chapter 1

Lightly Doped Semiconductors

This chapter is a short introduction to a basis of knowledge we need to be able to understand the problems of conductivity in strongly disordered materials like the lightly doped semiconductors. Before we dive into the discussions of disordered media it is worthy to pay the semiconductors a visit.

1.1 Energy Band Structure.

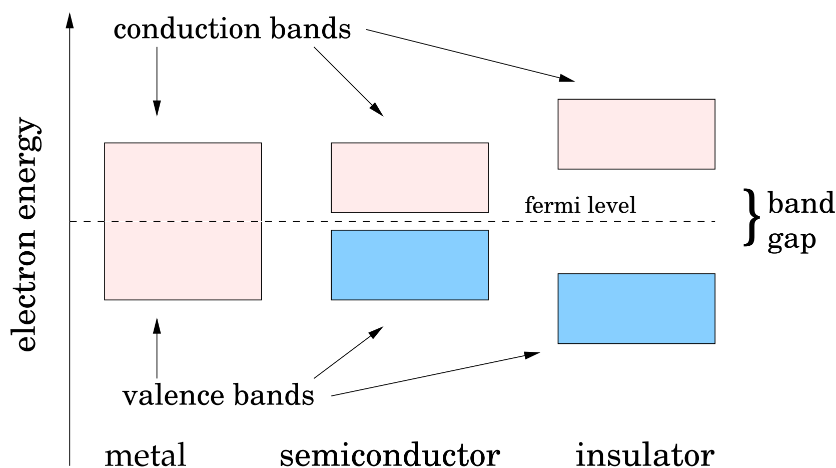

Figure 1.1: Schematic band structure of a metal with overlapping energy bands, a semiconductor with a narrow band gap, and an insulator with a wide band gap. Both the insulator and the semiconductor have completely filled valence bands and completely empty conduction bands in the ground state.

Every crystal contains electrons, but depending on how their electrons are arranged, determines if the solid is an insulator, a semiconductor or a conductor. An electron orbiting around an atom can be in different energy states, depending on the chemical element of the atom. When many atoms and their electrons are grouped together into a solid the energy states of all electrons will, by the Tight Binding Model, merge to continuous energy regions called the energy bands. The conduction band is the energy region where the electrons easily can conduct, whereas the valence band represents those orbitals in which the electrons are strongly bound to the atomic nucleus. There are also forbidden energy areas called band gaps in which the electron orbitals cannot exist. The gaps result from the interaction of the conduction electron waves with the crystal ions. In the band picture the crystal is an insulator if the energy bands in the ground state are either completely filled or empty and the gap between them is wide. If the band filling is the same as an insulator, but the gap is narrow, $E_{gap} << 2\ eV$, the material is a semiconductor. If there is no band gap the crystal is a metal[1]. The shape of the energy bands differ from material to material and require some effort to describe. This will not be discussed in further details, but can be easily found in the solid state literature [1]. For simplicity we use a schematic figure 1.1, which is enough for our purpose.

The most significant difference between metals, semiconductors and insulators are their transport properties. We are interested in investigating the semiconductors. Semiconductors can be classified as those solids that are insulating at $T = 0$, but whose band gaps are of such size that thermal excitation of carriers from the valence band to the conduction band can lead to observable current at temperatures above the absolute zero and below the melting point. In addition to the band gap the semiconductors have a negative coeficcient of resistance - their resistivity decreases as the temperature increases and this temperature dependence is strong. The semiconductors can either exist as perfect crystals or be disordered and have many structural faults. The former types are called crystalline and the latter amorphous semiconductors. The study of the inhomogenous semiconductors is useful since most of the materials are disordered. They occur in e.g electric devices used in our everyday life like the pn-junctions in the solar cells. They also contribute in the study of percolation transport in strongly disordered media. The crystalline semiconductors are convenient in the investigation of

[1]For orientation: The statement of a gapless material always being a metal is not completely true. There is a class of materials called gapless semiconductors, which will not be discussed further.

the fundamental principles of e.g band structure and doping. They are also widely used in heterostructure devices in transistors.

1.2 Doping and compensation.

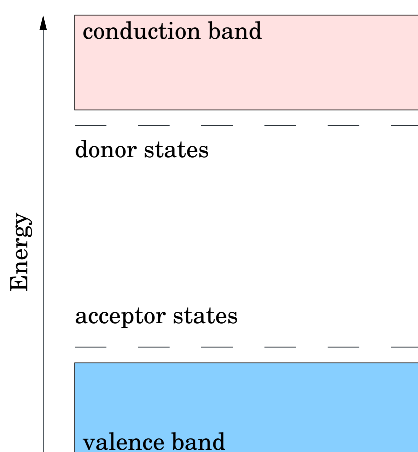

Figure 1.2: Schematic band structure of a doped, compensated semiconductor. The short lines represent shallow impurity energy states which are located close to the band edges: the donor states are close to the conduction band edge whereas the acceptor states are close to the valence band edge.

The electrical properties of a semiconductor can be drastically modified by embedding impurities into a pure semiconductor crystal, this is called doping. At high temperatures the impurities don't modify the electric properties of a semiconductor. There is enough thermal energy to bring valence electrons into the conduction band. This conduction type is called intrinsic. At low temperature most of the electronic properties of the doped semiconductors are determined by the impurities. There is not enough thermal energy to perform intrinsic conduction, but sufficient to establish impurity electron conduction. This is called extrinsic conduction. Depending on where the host crystal atoms and the impurities are located in the periodic table, the dopants can either act as donors - give away electrons, or act as acceptors - accept electrons. When all dopants are donors, the current carriers are negatively charged, hence the semiconductor is termed to be n-doped. The opposite situation happens in a p-doped semiconductor; the impurities accept electrons from the host lattice atoms and leave positively charged carriers,

holes, which propagate in the opposite direction of that the electrons would do.

If a mixture of donors and acceptors is embedded into the host lattice the semiconductor is compensated. The compensation factor K is the ratio of the amount of acceptors to the amount of donors $K = \frac{N_A}{N_D}$. The mixing contributes to charged particles in the system by the mechanism of donors giving away electrons to the acceptors. The system then has N_A negatively charged, ionized acceptor-impurities, N_A positively charged, ionized donor-impurities and $n = N_D - N_A$ negatively charged mobile electrons which can jump among the ionized donors. The motion of the electrons is affected by both the positive ionized donors and the negative ionized acceptors.

In addition to acting as donors and acceptors the impurities can further be categorised as either deep or shallow. An impurity is shallow if its energy level is close to one of the energy band edges as illustrated in figure 1.2. A deep impurity has its energy level located deep in the energy band gap. Our work is focused on the shallow impurities as they possess an important feature; their chemical properties almost don't influence the structure and energy of an impurity state. Their behavior is therefore possible to generalise into one theory:

It can be shown that the carriers coming from the shallow impurities are weakly bound to their hosts, have hydrogenic energy states and contribute to the transport in the material. This is shortly discussed in next subsection by the case of n-doping, which is the easiest to follow. In p-doping an equivalent situation arises, but with positive charge carriers.

1.2.1 The Hydrogenic Features of Dopants

We wish to know the shapes of the impurity electron wave functions and their energy states when they are put into a host crystal. A clever trick is to start considering the Hamiltonian of an electron in the vicinity of a single impurity which is embedded into a periodic lattice of a crystalline semiconductor. The main approach to this kind of problem is to start with something known and then to expand the solution. A well known problem solved by Bloch is the wave function of an electron in a periodic lattice. Detailed discussions on this can be found in any text book on solid state physics. Here only the results are taken advantage of and the discussion is brief. For more details see [2], chapter 1.

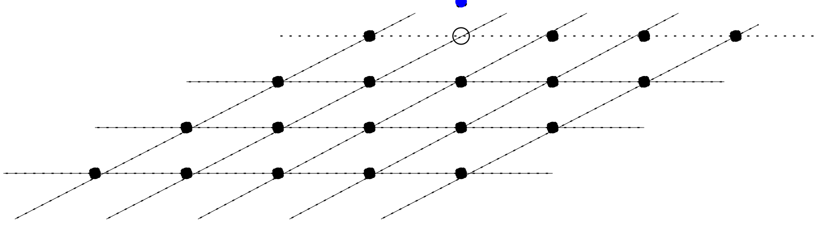

Figure 1.3: Schematic 2D picture of the system we wish to find electron wave functions for. The black dots are host crystal atoms, white dot represents the donor impurity, the blue dot is the donor electron. The figure is a zoom-in on an infinite lattice. Size proportions are not taken into account.

The system Hamiltonian in Bloch's problem is given by:

$$\mathcal{H}_0 = -\frac{\hbar^2}{2m_0}\nabla^2 + V(\mathbf{r}) \tag{1.1}$$

Where m_0 is the electron mass and $V(\mathbf{r})$ is the periodic lattice potential. The solution of the Schrödinger equation

$$\mathcal{H}_0|\phi\rangle = E|\phi\rangle \tag{1.2}$$

is provided by the Bloch functions

$$\phi(\mathbf{r})_{\mathbf{n},\mathbf{k}} \propto \mathbf{u}_{\mathbf{n},\mathbf{k}}\mathbf{e}^{\mathbf{k}\cdot\mathbf{r}} \tag{1.3}$$

(1.3) is a plane wave $e^{\mathbf{k}\cdot\mathbf{r}}$ modulated by a periodic function $u_{n,\mathbf{k}}$ with a periodicity of the host crystal lattice. Here $\mathbf{k}$ is a wave vector and n is the quantum number of the energy state.

By taking one dopant impurity with the potential $U(r) = \frac{e^2}{\kappa r}$ into account the Hamiltonian of the system in figure 1.3 is then:

$$\mathcal{H} = \mathcal{H}_0 + U(r) \quad = -\frac{\hbar^2}{2m_0}\nabla^2 + V(\mathbf{r}) + \frac{\mathbf{e^2}}{\kappa\mathbf{r}} \tag{1.4}$$

$U(r)$ is the Coulomb potential energy of the electron in vicinity of the impurity, e is the electron charge, κ is the dielectric permittivity of the lattice and r is the distance between the electron and the impurity. In reality this is a complex problem since the materials often have several conduction band

minima which also can be degenarate. However it is possible to make an estimate for the simplest case of a material with a standard band which has a single, non-degenerate conduction band minimum. For shallow impurities, which have their energy levels near the conduction band minimum at $\mathbf{k} \approx \mathbf{0}$ in the first Brillouin zone, we can make use of the "Effective Mass Approximation" method. The main idea of this approach is to assume that a motion of a particle of mass m_0 in some potential can for very small $\mathbf{k}$ be approximated with a motion of a free particle with an effective mass m with the kinetic energy of

$$E_n(k) = \frac{\hbar^2 k^2}{2m} \tag{1.5}$$

If the potential is strong, the electron is strongly affected and the effective mass is small. If the potential is weak, the motion of the particle is almost unaffected by it and the effective mass seems to be big. We also assume that at small $\mathbf{k}$ the energy is isotropic, meaning it is equal in all $\mathbf{k}$ directions: $E(\mathbf{k})= E(k)$ and we can then use the wave vector's length k in the calculations.

With the approximation in mind instead of using the Hamiltonian in (1.4) the following Schrödinger equation needs to be solved:

$$\Big[\frac{\hbar^2 k^2}{2m} + U(r)\Big]\Psi = E\Psi \tag{1.6}$$

It is further assumed that the wave function Ψ is some linear combination of Bloch functions and a function depending on the wave vector $\mathbf{k}$.

$$\Psi = \sum_{\mathbf{k}} B_n(\mathbf{k})\phi_{\mathbf{n},\mathbf{k}}(\mathbf{r}) \tag{1.7}$$

An extended calculation can be found in [2] chapter 1, with the result

$$\Psi(\mathbf{r}) = \mathbf{u_{n,0}}(\mathbf{r})\mathbf{F}(\mathbf{r}) \qquad F(\mathbf{r}) \sim \mathbf{e^{-r/a}} \tag{1.8}$$

$$E_n = -\frac{1}{n}\frac{e^2 a}{2\kappa} \tag{1.9}$$

The wave function of an impurity state is a Bloch wave function at the bottom of the conduction band $u_{n,0}$, $k = 0$, modulated by a large-scale hydrogen-like function $F(\mathbf{r}) \sim \mathbf{e^{-r/a}}$. Where $a = \hbar^2\kappa/me^2$ is the effective Bohr radius or

the loclization radius. This quantity estimates the attenuation length of a hydrogen-like localised wave-function. Typically in semiconductors the κ [2] is large and m is small. This results in a localization radius bigger than the lattice constant $a > \ell_0$. The localization radius can reach values of ~ 10 nm. The energy states E_n are by no surprise also hydrogenic and are shown in equation (1.9).

From this we see that an impurity electron has hydrogen-like wave function and energy states, its orbitals are far away from the donor center and the electron is weakly bound to it as shown in figure 1.4. Impurities are therefore easy to ionize and they strongly contribute to the current transport in the host material.

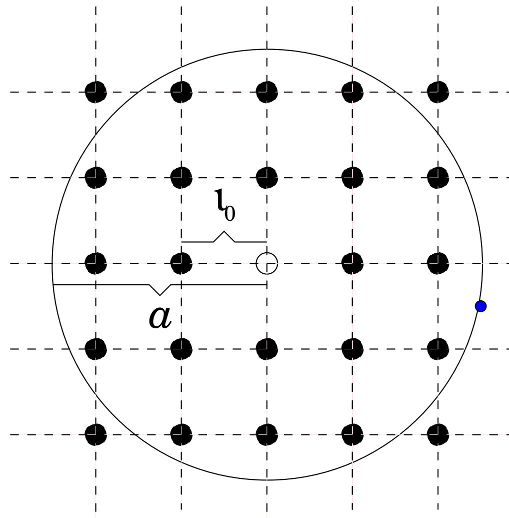

Figure 1.4: Schematic picture of a weakly bound donor electron orbiting the impurity with a much bigger radius - a than the lattice constant ℓ_0 of a semiconductor lattice.

[2]The static dielectric constants of semiconductors are large as a consequence of the small energy gaps. Without a gap the crystal would be a metal and κ would be infinite - meaning that a static electric field can induce a current in which electrons can move far from their original positions. A finite but large κ reflects an easy deformation of electrons' spatial distribution.[1]

1.3 Localization of Electronic States

In this section it is shortly described what happens in a system where many impurities reside in a host crystal and influence each other. As already seen every impurity has a hydrogen-like electron wave function which decreases exponentially with distance from the impurity. When there are many impurities in the system their wave functions might overlap with each other. If all the wave functions have a considerable overlap, all impurities should be able to share electrons. From the thorough studies done by Mott, Anderson and Lifshitz [2] there appear to exist certain conditions prohibiting a collective sharing of the electrons. This is called localization. A short explanation of the three models is given below.

Mott's localization model is constructed on a periodic impurity sublattice of identical atoms. By the tight-binding method the impurity energy levels merge into a so-called impurity band. This band doesn't behave as a regular energy band and its structure is unstable. Electron-electron interactions give rise to a splitting of the impurity band when the lattice constant is big. As long as the impurity band gap exists, the electronic states are localized. As the lattice constant is made smaller, at a certain point the gap vanishes and the sates become delocalized - or a Mott transition occurs.

Anderson's localization model also considers a periodic impurity sublattice, but there exists a disorder in the potential energy of the impurities. By quantum mechanics it can be shown that as long as two potential wells, representing the impurity potentials, are identical no matter the distance and overlap, an electron will be equally shared by the wells. As soon as there is a considerable potential difference, the electrons will be loacalized at their respective wells [2].

The Lifshitz model focuses on the positional disorder and gives a proof of a similar behavior as in the Anderson model only due to non-regular positioning of the impurities.

As it is seen, localization comes about either from disorder of some kind or from low impurity concentrations. Next chapter takes a closer inspection on how the localization affects the low temperature transport in lightly doped semiconductors.

Chapter 2

Conductivity in lightly doped semiconductors

At sufficiently low temperatures the transport in doped semiconductors is not due to free carriers but occurs as a result of charge transfer between impurity states. If the impurity concentration is high, the impurity states strongly overlap. In such case the electron wave functions are shared among all the impurities - which is called delocalization. It is then often said that an impurity band is formed and the conduction takes place in this "band". At low concentrations the impurity states have a small overlap, the electron wave functions are strongly localized and the conduction takes place by electron hopping from occupied to vacant localized donor states. We are interested in investigating hopping conduction in semiconductors in the hopping regime at low temperatures.

Figure 2.1 shows 4 temperature ranges where each area is characterised by its own conduction type. We focus on range A and D. They are most important when it comes to comparing electron transport through the conduction band at high temperatures with the hopping transport at low temperatures. The areas B and C will not be discussed in further detail in this thesis. The conduction of range A is characterised by thermal activation of electrons into the conduction band as shown in figure 2.2. As the temperature is decreased the semiconductor approaches area D where the hopping conduction begins. In the hopping temperature range there is not enough thermal energy to bring the electrons up to the conduction band. However, the available thermal energy can provide electron transport via small jumps on the empty impurity energy states inside the band gap as is shown in figure 2.3.

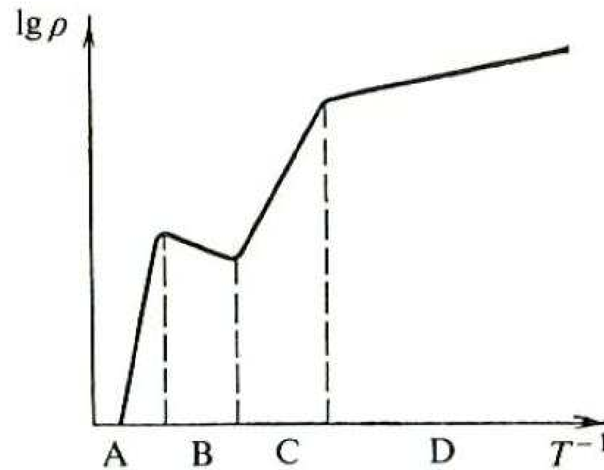

*Figure 2.1: The logarithm of resistivity as function of inverse temperature can be divided into 4 regions: A - Intrinsic conduction range.
B - Saturation range of impurity conduction.
C - Freeze out range, the free carriers are caught by the impurities.
D - Hopping range [2]*

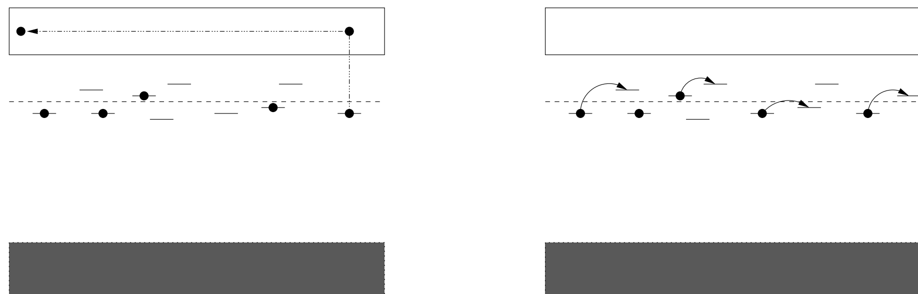

Figure 2.2: High temperature conduction mechanism: the electrons are lifted into the conduction band by the thermal energy.

Figure 2.3: Low temperature conduction mechanism: the electrons use the much smaller amount of thermal energy to jump among the impurity energy states.

The hopping range D can be further divided in two parts. In the leftmost part of the hopping range D in figure 2.1 the electron transport is mainly due to nearest neighbor jumps on the impurity energy levels in the semiconductor band gap. The jumps are activated by thermal energy often denoted by ε_3, which is constant down to some temperature limit. It is possible to show

that as the temperature is further decreased to the rightmost part of area D, the activation energy becomes temperature dependent $\varepsilon(T)$ and the average electron jumping length $\bar{r}$ will increase [2], [3]. This effect is usually referred to as Variable Range Hopping.

2.1 Hopping Conduction

Hopping was first suggested by Mott and Convell. Similar ideas were independently proposed by Pines, Abrahams and Anderson [5]. Miller and Abrahams developed the hopping rate where the jumps are governed by the phonon assisted tunneling and suggested the random resistor network model to describe the macroscopic hopping transport. The random resistor network problem can be solved by the percolation theory. Mott performed a further development of the Miller and Abrahams hopping rate and showed that by making a couple of assumptions a universal law for the hopping conductivity can be obtained. Efros and Shklovskii introduced Coulomb interactions into Mott's theory, which modify his original results. An extended discussion of the above concepts is given below.

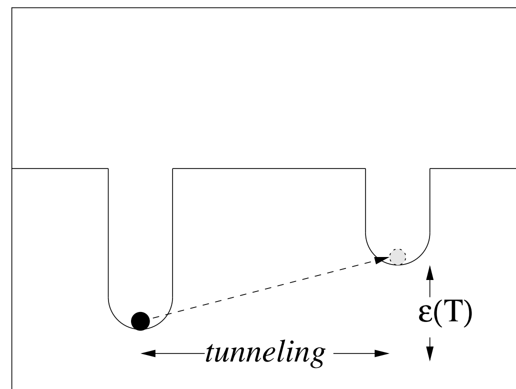

Figure 2.4: Phonon assisted tunneling. An electron can move to another impurity with help from quantum mechanical tunneling and thermal energy.

The idea of Miller and Abrahams builds on the following picture: Consider a lightly doped, compensated n-type semiconductor with a low dopant concentration in the temperature range D in figure 2.1. The compensation creates charged particles as described in section 1.2 with different site energies due to

the variations of local electric fields from ionized donors and acceptors. Low dopant concentrations result in small overlaps between the wave functions of neighboring impurity sites. The impurity energy disorder and low dopant concentration contribute to Anderson localization of the electron wave functions. If a donor electron is located close to another ionized donor, it can tunnel into this site. The transfer is accompanied by emission or absorption of a phonon with an energy of Δ_{ij}. Absorption or emission is to satisfy the energy conservation. This process is called *phonon assisted tunneling.* Figure 2.4 illustrates this kind of transfer. The hopping conduction is a result of many series of such transitions.

It is possible to calculate the probability (2.1) of an electron transition between the donors i and j and then to obtain the hopping rate (2.3) - the number of electron transitions per unit time, averaged over time. N is the phonon distribution function - Planck distribution, r_{ij} is the distance between a donor pair, a is the localization radius of the electron wave function and n_i , n_j are the donor occupation numbers.

$$\gamma_{ij} = \gamma_{ij}^0(\Delta_{ij}) \cdot e^{-2r_{ij}/a} \cdot N(\Delta_{ij}) \tag{2.1}$$

with

$$\gamma_{ij}^0 = \frac{E_1^2 \Delta_{ij}}{\pi \rho_0 \hbar^4 s^5} \Big(\frac{2e^2}{3\kappa a}\Big)\Big(\frac{r_{ij}}{a}\Big)\Big[1 + (\frac{\Delta_{ij} a}{2\hbar s})^2\Big]^{-4} \tag{2.2}$$

and

$$N_q(\Delta_{ij}) = \Big[e^{\Delta_{ij}/kT} - 1\Big]^{-1}$$

The hopping rate is then given by

$$\Gamma_{ij} = \langle\ \gamma_{ij}\ n_i(1 - n_j)\ \rangle_{\ t}\ . \tag{2.3}$$

A deeper discussion of the hopping rate derivation and an explanation to the symbols in (2.2) can be found in **Appendix A**. In the absence of an electric field there is a detailed balance in the charge transfer and therefore no net current. If a weak electric field is present, there will be more transitions against the field to sites of lower field energy than the opposite, and a net current proportional to the electric field will flow. An approximate evaluation of the current gives an expression for the resistance R_{ij} of a given donor pair. When many occupied and vacant donors are put together one

can picture the system as a network of random resistances. Below a short overview of Miller and Abrahams resistor network model is given.

The Random Resistor Network Model

The resistances are obtained by using *the self consistent field approximation.* This approximation is not trivial but turns out to be in accordance with many experimental results: The donor occupation numbers n_i fluctuate in time. This gives rise to variations in the donor potentials from which also Δ_{ij} also fluctuates. Hence γ_{ij} also fluctuates in time and is approximated by time averages of the occupation numbers $\langle n_i \rangle \equiv f_i^0$ and of the single particle energies $\langle \varepsilon_i \rangle \equiv \bar{\varepsilon}_i^0$. The weak electric field induces small changes in the averages

$$f_i = f_i^0 + \delta f_i, \qquad \bar{\varepsilon}_i = \bar{\varepsilon}_i^0 + \delta \varepsilon_i \quad .$$

These changes can be interpreted as a contribution to a local electrochemical potential drop $U_i - U_j$ between the two donors. Calculations in [2] show that the current can be expressed as

$$I_{ij} = -e(\Gamma_{ij} - \Gamma_{ji}) = \frac{1}{R_{ij}}\Big(U_i - U_j\Big) \tag{2.4}$$

with

$$R_{ij} = R_{ij}^0 \;\cdot\; e^{\xi_{ij}} \tag{2.5}$$

where

$$R_{ij}^0 = \frac{kT}{e^2\gamma_{ij}^0} \qquad \xi_{ij} = \frac{2r_{ij}}{a} + \frac{\epsilon_{ij}}{kT} \qquad \epsilon_{ij} = \frac{1}{2}\Big[|\bar{\varepsilon}_i - \bar{\varepsilon}_j| + |\bar{\varepsilon}_i - \mu| + |\bar{\varepsilon}_j - \mu|\Big] \;. \tag{2.6}$$

In a big sample there will be many pairs with a wide distribution of resistances which together constitute a network of random resistances similar to the one in figure 2.5.

The ideas and results of the phonon assisted hopping rate and the resistor network model had an important unanswered question; how to calculate the effective conductivity in such materials? Several problem solving suggestions were promoted. Averaging of the local conductance and the "chains and voids"-approach were the two most investigates ones. Unfortunately both were wrong. The former approach fails in only including the low resistances which seldom occur. This leads to calculation of the conductivity of small

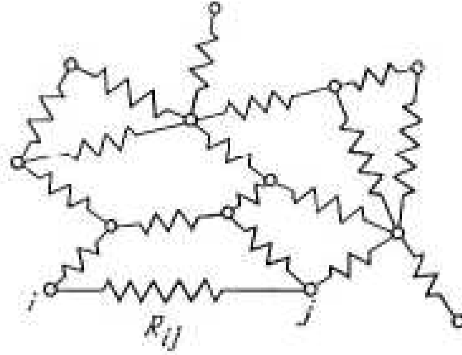

Figure 2.5: The Miller-Abrahams random resistor network as a model for the hopping conductivity [2].

conducting islands in a big insulating sea. The latter approach was based on the assumptions of a set of independent chains of resistances in series. These chains could break due to big voids - big distances between the impurity sites where the resistance is so large that no current can flow. In this model the current prefers voids of a certain radius which will dominate the resistances. The occurrence of such voids is also rather rare. By this approach one ends up with calculating the conductivity of dielectrical islands in a conducting sea. The final conclusion is: by these two methods the extremities of the effective conductivity are estimated. The common failure is; the methods overemphasize the role of anomalously rare resistances [2].

Then the light shone on, at that time, the brand new method of percolation, which turned out to be the key ingredient in solving the problem of the conductivity in a random resistor network.

2.2 Conductivity Through Percolation

The percolation theory was born in the 1950s and was introduced by Broadbent and Hammersley in connection with mathematical problems of liquid flow through a random labyrinth. Later it turned out that the concept of percolation could contribute in different fields like e.g. analogy to thermodynamics' treatment of second order phase transitions, correlation between ferromagnetic atoms in nonmagnetic hosts, polarization of ferroelectric materials, studies of the quantum Hall effect and hopping conductivity in disordered media. Percolation as a method of calculating the hopping conductivity

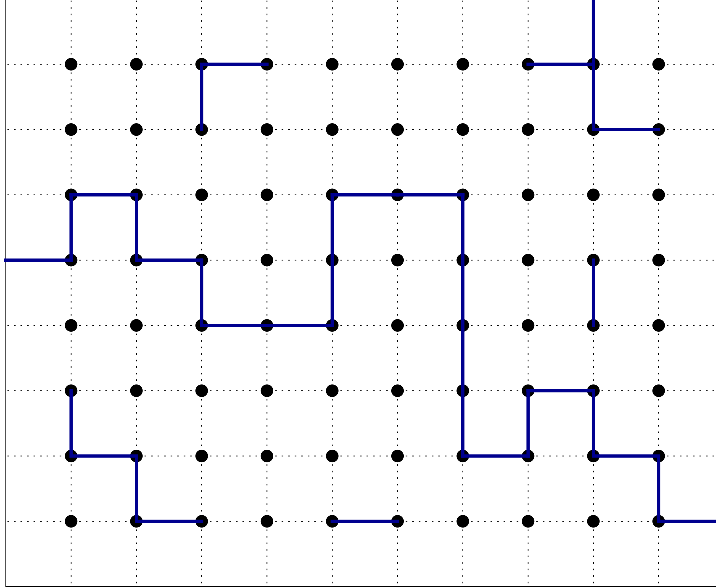

Figure 2.6: Illustration of the percolation bond problem where an infinite cluster takes form on a square lattice at the percolation threshold. The figure is a zoom-in on an infinitely large lattice.

in the random resistor network was independently proposed by Ambegaokar, Pollak, Shklovskii and Efros. Numerical experiments seem to agree well with the developed quantitative theory. In this chapter the most basic principles of the percolation theory are briefly discussed and an example on how to estimate the exponential factor of the effective hopping conductivity for a 2D simple square lattice is given.

The percolation problems can be divided into several groups: lattice site problems, bond problems, continuum problems and random site problems. They all share the same terminology but differ in details. Here we take a closer look at the bond problem which is easy to connect to the random resistor network model.

Bond problem of an infinitely large lattice.

Consider an infinitely large square lattice, a zoom-in of which is illustrated in figure 2.6. Between every lattice point there is a bond which can either be blocked or unblocked. If the bond between two sites is unblocked the lattice

points are connected. Otherwise the bond is blocked and there is no connection. Two important probabilities are introduced: x - the probability of an arbitrary bond being unblocked, or the fraction of unblocked bonds to the total amount of bonds. $P(x)$ - the probability that a random initial bond is unblocked and will interconnect infinitely many other unblocked bonds. Figure 2.7 shows the dependence of $P(x)$ on x. If x is small, there are few

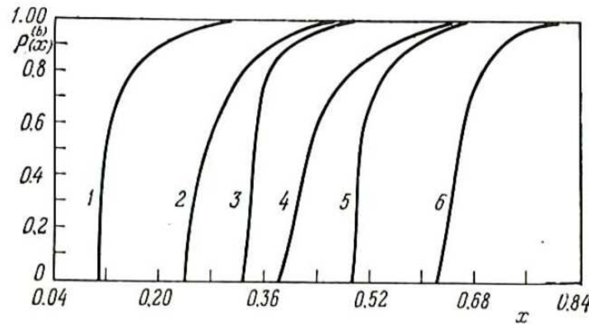

Figure 2.7: Probability $P(x)$ versus probability x for 6 lattice geometries in 2 and 3 dimensions. All are solved by the bond problem.
1 - face centered cubic, 2- simple cubic, 3 - triangular, 4 - tetrahedral, 5 - square, 6 - honeycomb [2], [4].

unblocked bonds, the probability of these being able to interconnect the entire sample is small, hence $P(x) = 0$. As x increases, more and more bonds get unblocked and form small isolated clusters which grow in size together with x.

At a certain value $x = x_c$ called the percolation threshold, there are finally enough unblocked bonds to establish a global, interconnecting bond chain. The previously small isolated clusters are big enough to reach each other and merge into an infinite cluster. The infinite cluster represents the random resistor network which permeates the entire space. The liquid in this case is naturally the electric current. $P(x)$ is equal to the ratio of the number of unblocked bonds in the infinite cluster to the total number of bonds and is the same as the density of the infinite cluster. $P(x)$ drastically increases right after the cluster is born. At $x > x_c$ but $x - x_c < 1$ the infinite cluster grows denser as it swallows more and more of the isolated islands. The growth slows down after $x - x_c >> 1$.

The above idea will now be connected to the random resistor network. An

estimate for the general exponential factor ξ_c of the effective electric conductivity $\sigma = \sigma_0 e^{-\xi_c}$ will be given. Our system is the simple square lattice in figure 2.6 with random resistances between adjacent sites. Let the lattice points represent the dopants. If the resistance is smaller than some selected value, the bond is unblocked. If the resistance is bigger than this value, it can be approximated to be infinitely large and the bond is blocked. $x = x(\xi)$ is now a function of the unblocked resistances, while $\xi \propto ln(\sigma)$ plays the role of $P(x)$.

From the result of Miller and Abrahams the resistance between two dopants is

$$R_{ij} = R_{ij}^0 \, e^{\xi_{ij}} \quad \xi_{ij} = \frac{2r_{ij}}{a} + \frac{\epsilon_{ij}}{kT}$$

We assume that the resistors in our system have uniformly distributed expo-

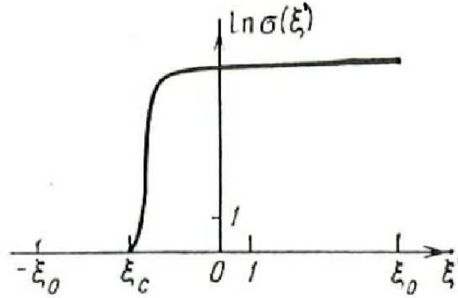

Figure 2.8: The logarithm of the resistivity versus the limit of the unblocked resistors. $ln\sigma$ and ξ play the role of $P(x)$ and x respectively [2].

nents in some interval: $-\xi_0 < \xi_{ij} < \xi_0$. We then choose to block all resistors with exponents bigger than some value $\xi^{'} \in (-\xi_0, \ \xi_0)$. The main task is to define the conductivity of the infinite cluster $\sigma(\xi_0) = \sigma(\xi^{'} >> \xi_c)$ when the largest resistances are gradually included into the network.

The probability of a bond being unblocked, x, depends on the choice of $\xi^{'}$ - which resistances are set to infinity, and its probability distribution $F(\xi)$.

$$x(\xi^{'}) = \int_{-\xi_0}^{\xi^{'}} F(\xi) \, d\xi \tag{2.7}$$

$F(\xi)$ is a uniform distribution function.

$$F(\xi) = \begin{cases} (2\xi_0)^{-1}, & |\xi| \leq \xi_0 \\ 0, & |\xi| \geq \xi_0 \end{cases} \tag{2.8}$$

From a straight forward integration of (2.7) the following $x(\xi)$ is obtained:

$$x(\xi) = \int_{-\xi_0}^{\xi'} \frac{1}{2\xi_0} d\xi = \frac{\xi_0 + \xi'}{2\xi_0} \tag{2.9}$$

From figure 2.8 it is seen that when ξ' is close to $-\xi_0$, $x \approx 0$. The few unblocked resistances form isolated clusters, but the overall conductivity is 0. As x increases linearly with ξ' the number of unblocked bonds grows. At the percolation threshold $\xi' = \xi_c$, x is by (2.9) equal to

$$x_c = \frac{\xi_0 + \xi_c}{2\xi_0} \tag{2.10}$$

and an infinite cluster is formed. As long as $0 < \xi' - \xi_c \leq 1$ is true, the newly formed cluster is called the critical sub-network. As long as we are in the critical sub-network and include larger resistors, the change in $\sigma(\xi')$ will still be negligible:

$$\sigma(\xi_c + 1) \propto \sigma_0 \; e^{\xi_c} \tag{2.11}$$

This is an important result: The conductivity of a random resistor network is determined by the resistances belonging to the critical sub-network which is established at the percolation threshold. Even though the infinite cluster density increases and bigger resistances are included, they will not alter the σ significantly, because the current always chooses the path of lowest possible resistance. This path is defined by the critical sub-network.

To sum up; if the elements of a medium are turned on in the order of increasing resistance, the effective conductivity's exponential factor ξ' is determined by those elements that first create an interconnected percolation path, and $\xi' = \xi_c$.

Particular expressions for ξ_c depend on the chosen percolation model and how the wave functions of the dopants are modeled.

Percolation seems to be a good approach for solving the random resistor network model. What must be kept in mind is the foundation of the model;

the time averaging of the single particle energies and the occupation numbers which lead to the concept of a resistance between two donors.

2.3 Mott's Law and Variable Range Hopping

Sir Nevill Mott was one of the first to give a theoretical description of the low temperature hopping conductivity in strongly disordered systems with localized states based on the Miller and Abrahams hopping rate [3]. In 1969 he introduced the concept of Variable Range Hopping - how the long jumps govern the conductivity at sufficiently low temperatures.

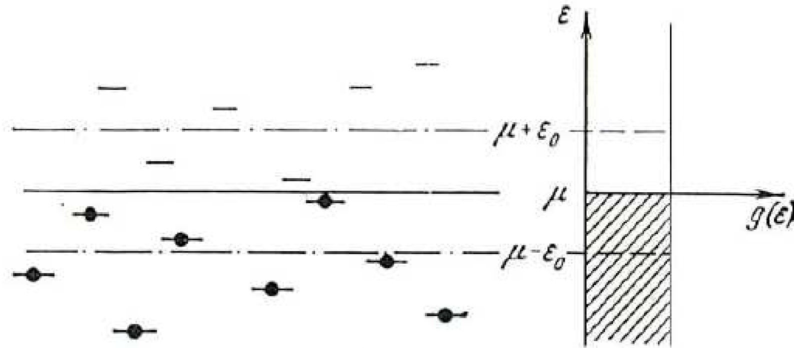

Figure 2.9: Schematic figure of a constant density of states in a small energy interval of $2\varepsilon_0$ centered on the Fermi level μ. The system is in the ground state. No Coulomb interactions are taken into account [2].

His assumptions and approximations have later been pointed out to be of a too simple kind and suggested improvements to his theory appeared throughout the subsequent decades. Mott's ideas are shortly discussed below.

Mott's theory makes the assumption of a constant density of states in vicinity of the Fermi level, $g(\varepsilon) = g(\mu)$, as shown in figure 2.9. This means that the Coulomb interactions between the particles are not taken into account. At low temperatures the conductivity then shows a universal behaviour. In the below discussion a general derivation of the conductivity $\sigma(T)$ and the average jumping length $\bar{r}(T)$ in d dimensions is given based on the discussion in [2].

The concept of variable range hopping can be explained as the electron ten-

dency to favour a more spatially distant site with a smaller hopping energy requirement than a close site with a big energy requirement. Mott explained the qualitative concept of Variable Range Hopping by phonon assisted tunneling, on which the Miller-Abrahams resistor network model [5] is based.

As the temperature decreases it will be shown that the available thermal activation energy $\varepsilon_0(T)$ in (2.17) also decreases. This means that only the electrons with energy states close to the Fermi level μ are allowed to jump. The prize of a jump from an occupied to an empty impurity state an electron can afford, is the energy $\varepsilon_0(T)$. Empty energy states which are $\varepsilon_0(T)$ or closer to μ are quite rare and are separated by greater spatial distance. The lower the temperature is, the fewer energetically affordable sites there are, and the bigger is their spatial separation. Therefore the jump lengths increase as the temperature decreases.

The derivation of $\sigma(T)$.

We now look at a small energy interval of width $2\varepsilon_0$ centered around the Fermi level as shown in figure 2.9. With a constant density of states the number of energy states within this interval, when omitting the factor of 2, is then

$$N(\varepsilon_0) \approx g(\mu)\varepsilon_0 \tag{2.12}$$

The conductivity resulting from hopping on impurity levels within the energy interval can be established by a very crude approximation: Assume that all pairs within this interval have an average energy difference of $\varepsilon_{ij} = \varepsilon_0$ and an average jumping length of $r_{ij} = \bar{r}$. The hopping resistivity is then given by

$$\rho = \rho_0 \; exp \left[\frac{2\bar{r}}{a} + \frac{\varepsilon_0}{kT}\right] \tag{2.13}$$

Now a short explanation to the following calculations will be given: There is a competition between the two terms in the brackets of (2.13) on whether the overlap of the wave functions or the thermal activation energy will dominate the resistivity. By expressing both terms in the brackets in terms of ε_0, differentiating them with respect to ε_0 and equating the sum to zero, the minimum of the resistivity exponent can be found. This corresponds to a situation where there is an equal contribution to the resistivity from thermal activation and from tunneling between the sites. We further find $\varepsilon_0(T)$ of

this minimum and insert it back into equation (2.13). From this a general expression of the temperature dependent hopping conductivity is obtained:

Substitute

$$\bar{r} = N(\varepsilon_0)^{-1/d} \approx (g(\mu)\varepsilon_0)^{-1/d} \tag{2.14}$$

into (2.13). When omitting non important numerical constants the exponential factor of (2.13) is then

$$\frac{1}{a(g\varepsilon_0)^{1/d}} + \frac{\varepsilon_0}{kT} \tag{2.15}$$

Differentiating equation (2.15) with respect to ε_0 and searching for the minimum gives:

$$\frac{\partial}{\partial\varepsilon_0}\left(\frac{1}{a(g\varepsilon_0)^{1/d}} + \frac{\varepsilon_0}{kT}\right) = -\frac{\varepsilon_0^{-((1+d)/d)}}{adg^{1/d}} + \frac{1}{kT}$$

$$-\frac{\varepsilon_0^{-((1+d)/d)}}{adg^{1/d}} + \frac{1}{kT} = 0 \tag{2.16}$$

Rearranging with respect to ε_0 and neglecting the factor $d^{d/d+1}$ in the denominator, we obtain

$$\varepsilon_0(T) \approx \left(\frac{(kT)^d}{a^d g(\mu)}\right)^{\frac{1}{d+1}} \tag{2.17}$$

This expression shows that the activation energy is temperature dependent and decreases with decreasing temperature. When substituting the expression (2.14) and (2.17) into (2.13) one obtains

$$\rho(T) = \rho_0 \ \exp\left[\left(\frac{T_0}{T}\right)^p\right] \Longleftrightarrow \sigma(T) = \sigma_0 \ \exp\left[-\left(\frac{T_0}{T}\right)^p\right] \tag{2.18}$$

with

$$p = \frac{1}{d+1} \qquad T_0 = \frac{\beta}{kg(\mu)a^d} \tag{2.19}$$

β in (2.19) is a numerical coefficient containing all the omitted prefactors in the exponent in addition to the unknown prefactor of the density of states $g(\mu)$. In 3 dimensions $p = \frac{1}{4}$. Mott's law for the hopping conductivity is therefore often denoted as the $T^{-\frac{1}{4}}$ - law.

The derivation of $\bar{r}(T)$.

It is now straight forward to show that the average jumping length increases with decreasing temperature as

$$\bar{r} \sim T^{-p}. \tag{2.20}$$

Where p is the same exponent as in (2.18). From (2.14) we see that $\bar{r}(\varepsilon_0)$ is temperature dependent, since $\varepsilon_0(T)$ in (2.17) is temperature dependent. We insert (2.17) into (2.14) and obtain

$$\bar{r} = [\varepsilon_0(T)g(\mu)]^{-1/d} \approx \Big(\frac{a}{gkT}\Big)^{\frac{1}{d+1}} = \frac{a}{(gka^d)^{1/d+1}} \cdot \frac{1}{T^{1/d+1}} \quad . \tag{2.21}$$

Including T_0 from (2.19) we see that the average jumping length increases with decreasing temperature.

$$\bar{r} \approx a \cdot \Big(\frac{T_0}{T}\Big)^{\frac{1}{d+1}} \approx a \cdot \Big(\frac{T_0}{T}\Big)^p \tag{2.22}$$

2.3.1 Discussion on the Assumptions in Mott's Law

Mott's work is based on the Miller and Abrahams hopping rate with a couple of crude approximations in the derivation. The first and the most crucial one is the assumption of a constant density of states near the Fermi level, which means there are no interactions between the particles. Experiments and theoretical work show that at sufficiently low temperatures there occurs a depletion of the density of states near the Fermi level, called the Coulomb gap. The gap is caused by the Coulomb interactions between the charged particles and has a major effect on the conductivity. Next there is the assumption of all pairs having equal energy difference $\varepsilon_{ij} = \varepsilon_0$, and all jumps having an average length $\bar{r}$, which is also not completely true with respect to the interactions. In the next two sections it will be shown how an adjustment of these assumptions results in a different $\sigma(T)$ expression.

However Mott's theory was an enormous breakthrough in the late 1960s. In many materials like amorphous semiconductors the structural defects is the main type of disorder and the Coulomb gap is smeared out. In these materials the experimental results are best described by Mott's law. Smearing of the gap can also happen due to increased temperature. Which means that systems with weak structural disorder are then better described by Mott's

law. The improved model discussed in the coming sections 2.4 and 2.5 is thus relevant in high-quality materials with a weak structural disorder at sufficiently low temperatures.

2.4 The Coulomb Gap

Mott's Variable Range Hopping theory was brought further and adjusted by including Coulomb interactions between the charged particles within the system. When the strong interactions are taken into account, a different situation than what predicted by Mott's law arises. The ground state electronic density of states vanishes at the Fermi level. This is called the Coulomb gap and is illustrated in figure 2.10. At zero temperature the density of states will be zero at the Fermi level. As the temperature rises the gap is smeared out due to fluctuations. The Coulomb gap strongly affects the behavior of the conductivity. The hopping transport appears to be more complex than in a similar system without interactions. Every jump changes the charge configuration and the single particle energies of the whole system. Hamilton and Pollak were one of the first to consider the non-constant density of states. Their results were later improved by Efros and Shklovskii [2] and give a new conductivity relation. In this section we take a look at the manifestation of the Coulomb gap and show that figure 2.10 depicts its shape. The conductivity when including the Coulomb interactions will be discussed in next section.

The Coulomb Gap (CG) in the density of states occurs due to the strong Coulomb Interaction (CI) between the electron energy states close to the Fermi level. Assume the system is in its ground state. All electron energy states below the Fermi level μ are then occupied while all the states above μ are empty, as shown in figure 2.11. Any electron transfer from an energy state $\varepsilon_i < \mu$ to $\varepsilon_j > \mu$ must give a positive energy change, since the ground state is the lowest energy state. Equation (2.23) shows the change in energy due to a single electron jump. This is the required work to transfer an electron from site i to j. Equation (2.24) is the expression for single particle energy. The single particle energy ε_i depends on the site potential U_i and on the Coulomb interactions from all the surrounding sites in the system.

$$\Delta E_{i \to j} = \varepsilon_j - \varepsilon_i - \frac{e^2}{\kappa r_{ij}} > 0 \tag{2.23}$$

$$\varepsilon_i = U_i + \sum_{j \neq i} \frac{e^2}{\kappa r_{ij}} \tag{2.24}$$

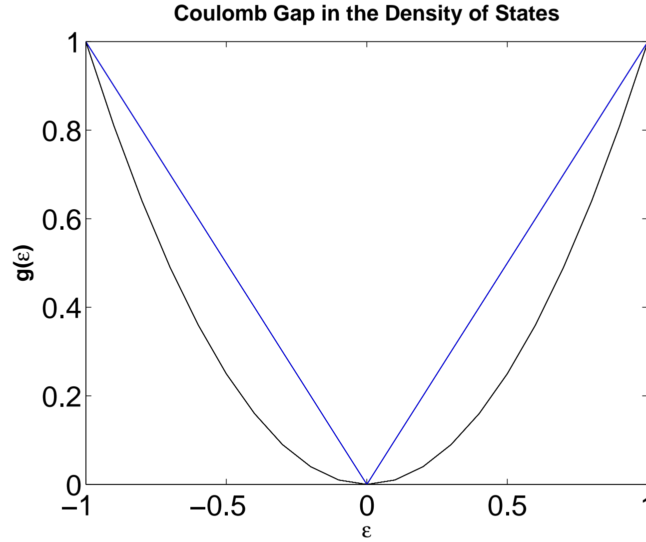

Figure 2.10: The Coulomb Gap in the density of states. The linear graph shows the gap formation in 2D. The parabolic graph shows the gap in 3D.

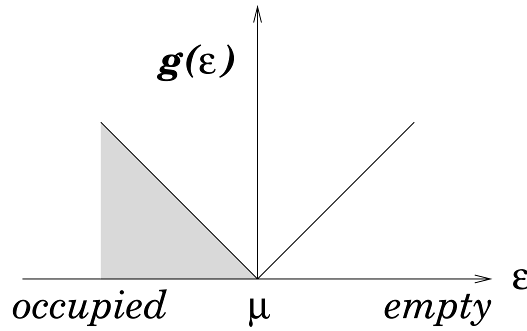

Figure 2.11: Coulomb gap in the density of states in 2 dimensions. In the ground state the states below the Fermi level μ are occupied, whereas the ones above are empty.

To remove the electron from site i the energy of $-\varepsilon_i$ is needed. To bring the electron onto the site j the amount of work $\varepsilon_j - \frac{e^2}{\kappa r_{ij}}$ must be done. The $-\frac{e^2}{\kappa r_{ij}}$ term is included to compensate for the interaction from the now empty donor on site i while bringing the electron onto the site j. In other words; the self interaction of the electron with itself on its old site i is avoided by

subtracting $\frac{e^2}{\kappa r_{ij}}$. A further discussion on the change in energy due to an electron jump in the presence of an electric field will be picked up in chapter 3, The Coulomb Glass Model.

Consider again a small energy interval ε_0 centered around μ. We see from (2.23) that any two nonempty and empty sites with energies within this interval must be separated by a distance bigger than $r_{ij} > e^2/\kappa\varepsilon_0$.

$$
\begin{aligned}
\varepsilon_j - \varepsilon_i - \frac{e^2}{\kappa r_{ij}} &> 0 \quad \varepsilon_j = \frac{\varepsilon_0}{2} \quad \varepsilon_i = -\frac{\varepsilon_0}{2} \\
\rightarrow \quad \varepsilon_0 &> \frac{e^2}{\kappa r_{ij}} \\
\rightarrow \quad r_{ij} &> \frac{e^2}{\kappa\varepsilon_0}
\end{aligned} \tag{2.25}
$$

The closer the energies of ε_i and ε_j are to μ, the bigger must the spatial distance between these states be. Equation (2.23) gives that the number of donors within a volume with radius r_{ij} can't exceed one. The concentration of donors with energies $|\varepsilon - \mu| < \varepsilon_0$ in d dimensions is then given by

$$
n(\varepsilon_0) = \frac{1}{r(\varepsilon_0)^d_{ij}} = (\frac{\kappa\varepsilon_0}{e^2})^d \; . \tag{2.26}
$$

From this it follows that the density of states

$$
g(\varepsilon_0) = \left|\frac{\partial n(\varepsilon_0)}{\partial\varepsilon_0}\right| = d(\frac{\kappa}{e^2})^d \varepsilon_0^{d-1} \tag{2.27}
$$

cannot be constant in 2 and 3 dimensions as the energy approaches μ. In 3 dimensions we see that the gap is parabolic $g(\varepsilon_0) \sim |\varepsilon_0 - \mu|^2$, whereas in 2 dimensions the gap should be linear $g(\varepsilon_0) \sim |\varepsilon_0 - \mu|^1$, as shown in figure 2.10. A general density of states affected by Coulomb interactions can be denotes as

$$
g(\varepsilon) \propto |\varepsilon - \mu|^n \; . \tag{2.28}
$$

2.5 The Efros - Shklovskii Law

It is now possible to use the result of the vanishing density of states (2.28) in the same kind of derivation of conductivity as in section 2.3. Below a

general expression of how p depends on the shape of the density of states $g(\varepsilon)$ and the spatial dimension d is given. The final result is often called the Efros-Shklovskii $T^{-1/2}$ law which estimates hopping conductivity when the Coulomb interactions are taken into account.

We again start with the expression of the resistivity and concentrate on the exponent.

$$\rho \propto \exp\left[\frac{2\bar{r}}{a} + \frac{\varepsilon}{kT}\right] \sim \exp\left[\left(\frac{T_0}{T}\right)^p\right], \quad 0 < p < 1 \tag{2.29}$$

Since the main importance is the behaviour of the exponent and its exponent p, we can avoid paying attention to the constants and prefactors throughout the derivation. They will be omitted. In resemblance with the approach in section 2.3 we express both terms in the brackets of (2.29) by ε, find exponent's minimum, and insert the expression of $\varepsilon(T)$ into equation (2.29). This results in an expression of the exponent from which we can define an expression for p. Below the details on the calculations are given:

We substitute the average distance between the lattice sites $\bar{r}$ to $\bar{r} = N(\varepsilon)^{-\frac{1}{d}}$ in a d-dimensional system. From calculations in [2] chapter 9, it can be seen that for a density of states $g \propto |\varepsilon - \mu|^n$ we get an expression for the concentration of electrons $N(\varepsilon)$ to be

$$N(\varepsilon) = \int_{\mu-\varepsilon}^{\mu+\varepsilon} g(\varepsilon)\, d\varepsilon \;\sim\; \varepsilon^{n+1} \tag{2.30}$$

In order to simplify the expressions the Fermi level is set to the origin, $\mu = 0$. We then substitute the expression $N(\varepsilon) \sim \varepsilon^{n+1}$ into equation (2.29).

$$\rho \sim exp\left[N(\varepsilon)^{-\frac{1}{d}} + \frac{\varepsilon}{kT}\right] \sim exp\left[(\varepsilon^{n+1})^{-\frac{1}{d}} + \frac{\varepsilon}{kT}\right] \tag{2.31}$$

Differentiating and equating the exponent to zero with respect to ε gives

$$\begin{aligned} \frac{\partial}{\partial\varepsilon}\left[(\varepsilon^{n+1})^{-\frac{1}{d}} + \frac{\varepsilon}{kT}\right] &= 0 \\ -\frac{1}{d}(\varepsilon^{n+1})^{-\frac{1}{d}-1}(n+1)\varepsilon^n + (kT)^{-1} &= 0 \\ \varepsilon &\sim (kT)^{\frac{d}{n+d+1}} \end{aligned} \tag{2.32}$$

Inserting the new expression (2.32) into the equation (2.31) gives us the exponent of the resistivity:

$$
\begin{aligned}
\left(\varepsilon^{n+1}\right)^{-\frac{1}{d}} + \frac{\varepsilon}{kT} &\sim \left(kT\right)^{\left(\frac{d}{n+d+1}\right)\left(n+1\right)\left(-\frac{1}{d}\right)} + \left(kT\right)^{\frac{d}{d+n+1}-1} \\
&\sim 2\left(kT\right)^{-\left(\frac{n+1}{n+d+1}\right)} \\
&\sim \left(\frac{T_0}{T}\right)^{\frac{n+1}{n+d+1}}
\end{aligned}
\tag{2.33}
$$

From this we see that we have a general expression which states that

$$
\rho(T) = \rho_0 \ \exp\left[\left(\frac{T_0}{T}\right)^p\right] = \rho_0 \ \exp\left[\left(\frac{T_0}{T}\right)^{\frac{n+1}{n+d+1}}\right]
$$

Then

$$
p = \frac{n+1}{n+d+1} \tag{2.34}
$$

In 2 dimensions with $d = 2$ and $n = 1$ or for 3 dimensions with with $d = 3$ and $n = 2$, $p = \frac{1}{2}$. Hence the resistivity and the conductivity are given by

$$
\rho_{CI}(T) = \rho_0 \ \exp\left[\left(\frac{T_0}{T}\right)^{1/2}\right] \Longleftrightarrow \sigma_{CI}(T) = \sigma_0 \ \exp\left[-\left(\frac{T_0}{T}\right)^{1/2}\right] \tag{2.35}
$$

2.6 Non-Ohmic Variable Range Hopping

The problem of electron transport in strong fields was already discussed in the 1960s and 1970s by Mott, Sayer, Austin, Reik and many more [6]. The discussion of charge transport in strong fields can be divided in two:
1) the mobility of a single carrier and 2) the conductivity of a degenerate electron gas when the Variable Range Hopping occurs. Both 1) and 2) have been discussed throughout the years and there is still an ongoing development in this area. In case 1) the focus is on investigating whether the carrier mobility is governed by the formation of polarons[1], or if it is governed by

[1]Polaron is a quasi particle composed of an electron and its accompanying polarization field. A slow moving electron in a dielectric crystal, interacting with lattice ions through long-range forces will permanently be surrounded by a region of lattice polarization and deformation caused by the moving electron. Moving through the crystal, the electron carries the lattice distortion with it, thus one may speak of a cloud of phonons accompanying the electron.

geometrical traps in the lattice [6], [7].

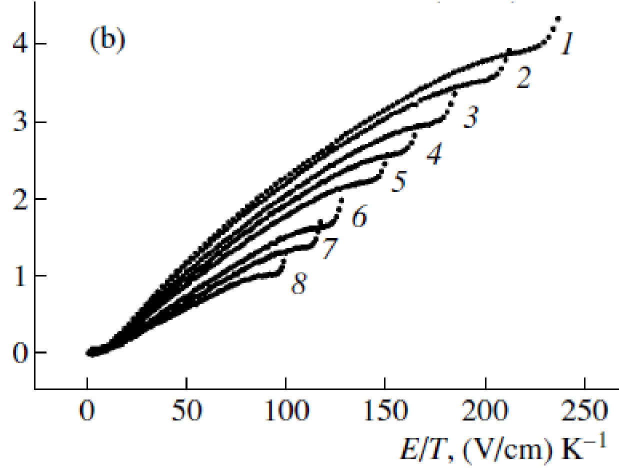

Figure 2.12: Field dependencies of the logarithm of the structure conductance as a function of E/T at 8 different temperatures: 1) 4.22K, 2) 4.7K, 3) 5.4K, 4)6.0K, 5)6.6K, 6)7.8K, 8)10K. Aronzon et al, [8]. $\sigma(E) \propto E$ seems to be a good weak field description. σ_0 is the conductance in the Ohmic limit. Aronzon et al. [8]

When it comes to the research of 2) there are several theoretical models predicting the following dependencies [8]:

$$ln\sigma(E) \propto E^{1/2} \quad ln\sigma(E) \propto E \quad ln\sigma(E) \propto E^2$$

The experimental studies of a quasi 2D hopping conductance channel formed in a MOSFET structure done by Aronzon et al. [8] are displayed in figure 2.12 and 2.13. The figures show two plots; $ln(\sigma/\sigma_0)$ versus $E^{1/2}/T$ and $ln(\sigma/\sigma_0)$ versus E/T. In the non-Ohmic field region the measurements in figure 2.12 don't collapse, while the measurements in figure 2.13 collapse and fit with a fairly straight line for the relation $ln\sigma(E) \propto E^{1/2}/T$. In chapter 5 we discuss our numerical results in the non-Ohmic regime and compare our simulation data to the relation

$$\sigma(E,T) = \sigma_0 \exp\Big(\alpha\frac{E^{1/2}}{T}\Big), \quad \alpha = constant \tag{2.36}$$

and the results of Aronzon et al.

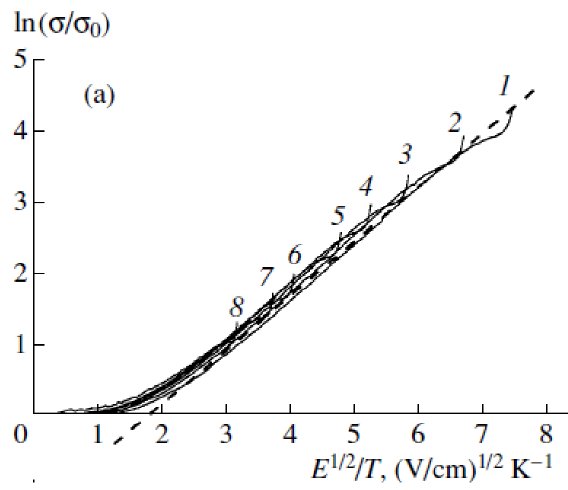

Figure 2.13: Field dependencies of the logarithm of the structure conductance as a function of $E^{1/2}/T$ *at 8 different temperatures: 1) 4.22K, 2) 4.7K, 3) 5.4K, 4)6.0K, 5)6.6K, 6)7.8K, 8)10K. Aronzon et al.* $\sigma(E) \propto E^{1/2}$ *seems to be a good description for strong fields to a certain limit.* σ_0 *is the conductance in the Ohmic limit. Aronzon et al. [8]*

Chapter 3

The Coulomb Glass Model

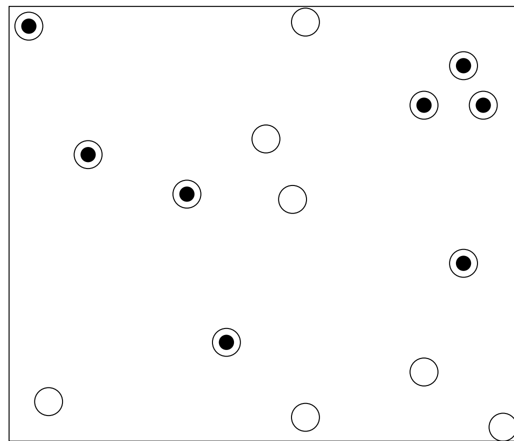

Figure 3.1: Lightly doped semiconductor with positional disorder. The impurities (white circles) are randomly embedded into the host material. Some of the sites posses an electron (black circles).

Coulomb Glass Systems and materials

The Coulomb Glass model was originally developed for lightly doped, compensated semiconductors in the 1960s. Since then the model has been widely applied to most systems where the electron wave functions are localized by disorder and where there is an indication of a Coulomb Gap. Amorphous semiconductors, alloys, doped conducting polymers and granular films under certain circumstances, are examples of materials where the Coulomb Gap manifests itself. Evidence of the Coulomb Gap in two dimensions has

also been found in field effect transistors (MOSFETs) and Gallium Arsenide hetero-structures. In addition the model can apply to correlated transport of vortices in superconductors and to biological systems concerning protein folding [9]. More details can be found in the review of M.Ortuño et. al. [10].

A common feature of Coulomb glass systems is their localised states, which are caused by system disorder of some kind, and strong long-range Coulomb interactions between the charged particles within the system. In semiconductors at low temperature the creation of charged particles happens as a result of compensation discussed in section 1.2. Carrier dynamics in a landscape with a varying potential is the main focus of experimental and theoretical studies. Equation (3.1) shows the single-particle energy ε_i of an impurity in such Coulomb glass systems.

$$\varepsilon_i = U_i + \sum_{j \neq i} \frac{(n_i - \nu)(n_j - \nu)}{r_{ij}} \tag{3.1}$$

The dielectric constant κ and the electric charge e are set to unity. As already discussed in section 2.4, all impurities posses their own potential energy U_i, also denoted as disorder energy, and are affected by Coulomb interactions from all other charged sites in the system. n_i , n_j are the site occupation numbers. If a site i possesses an electron, $n_i = 1$. If the site is empty, $n_i = 0$. The $\nu = 0.5$ is an average charge number and is necessary in inclusion of the interactions between both positive and negative charges and to preserve the neutrality of the system. By doping the host crystal with a compensation of $K = 0.5$ there are twice as many donors as there are acceptors. All acceptors absorb a donor electron and are negatively charged whereas the ionized donors are positively charged. The $n = N_D - N_A$ electrons can then jump among the ionized, positively charged donors while they are influenced by the Coulomb interactions from the negatively charged acceptors. On average the sample is neutral with the average charge of 0.5 as mentioned in section 1.2.

The fact that every single-particle energy is affected by the specific charge configuration in its environment adds complexity to the system. Equation (3.2) is the system Hamiltonian with no electric field present.

$$\mathcal{H} = \sum_i n_i U_i + \frac{1}{2} \sum_{i,j} \frac{(n_i - \nu)(n_j - \nu)}{r_{ij}} \tag{3.2}$$

The total energy of the Coulomb glass naturally depends on the disorder energies U_i and the interaction energy between all the charged particles. The

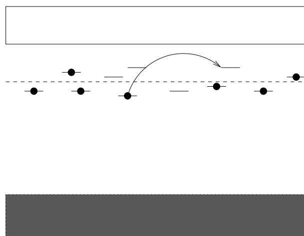

Figure 3.2:

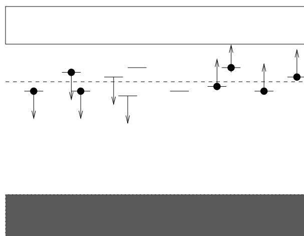

Figure 3.3:

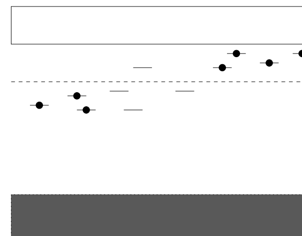

Figure 3.4:

latter is decided by their charge and spatial configuration. This implies that when a jump is made, the charge configuration is changed, which modifies all single particle energies ε_i and hence also the total energy of the system. This contributes to a more intricate type of electron dynamics where the impurity energy levels within the band gap are slightly altered after every jump. The alteration depends on the dopant-electron configuration in question. Figures 3.2, 3.3 and 3.4 illustrate the impurity energy shifts due to one electron jump: Figure 3.2 shows the energy levels of some configuration before an electron jumps. Figure 3.3 and 3.4 show how the impurity energy levels shift after a jump. If an electron jumps to an area with other occupied sites nearby, repulsion will occur. The local Coulomb potential of all sites in this area increases and makes it more difficult to enter for another electron. At the same time, the area the electron left now has a positively charged hole and the Coulomb potential is lowered a bit. This positively charged spot is attractive for another electron to settle down in.

In this thesis a semiconductor system under influence of an electric field is investigated. The system Hamiltonian obtains an additional electric field term compared to equation (3.2). This term describes the potential energy all charged particles obtain in the presence of the field.

$$\mathcal{H} = \sum_i n_i U_i + \frac{1}{2} \sum_{i,j} \frac{(n_i - \nu)(n_j - \nu)}{r_{ij}} + \sum_i n_i \vec{r_i} \cdot \vec{E} \tag{3.3}$$

$$\Delta E_{i \to j} = \varepsilon_j - \varepsilon_i - \frac{1}{r_{ij}} + \vec{r_{ij}} \cdot \vec{E} \tag{3.4}$$

Equation (3.4) is an extended version of equation (2.23) and shows the change in energy due to a single electron jump in the presence of an electric field.

3.1 The lattice model

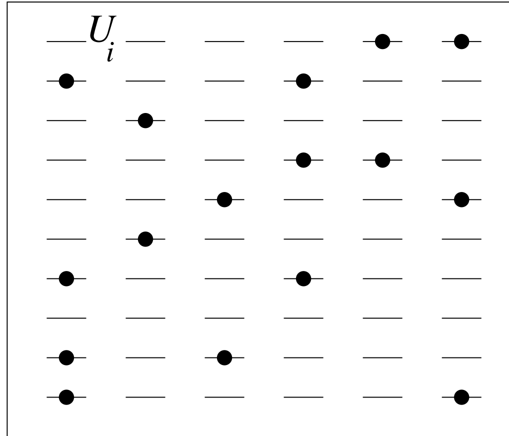

Figure 3.5: A zoom in on the model of a square lattice with $L \times L$ impurities and $0.5 \cdot (L \times L)$ mobile carriers. The lines represent the positively charged impurities. The black dots represent the electrons which are allowed to jump on the impurities.

Our lattice model represents a system of a general, lightly n-doped semiconductor of intermediate compensation which is in contact with a huge phonon bath reservoir as shown in figure 3.5. We consider a two dimensional square lattice with $L \times L$ lattice sites which represent positively charged impurity dopants. Every impurity is in possession of its own disorder potential energy U_i. The disorder energies are randomly chosen from a uniform distribution within an interval of $U_i \in [-1, 1]$. The regularity of the impurity positions doesn't exactly resemble the situation in real materials, where the impurities have some level of positional disorder. The purpose of the impurity lattice is mainly to decrease the computational time. Also - similar computations done with different lattice geometries have shown that the results are lattice invariant.

Half of the sites are initially randomly filled with negatively charged electrons. All impurities are fixed in space, but the electrons are mobile and can pass from one impurity to another.

We use Coulomb energy units, which means that an interaction energy of two electrons on nearest neighbour sites $r_{ij} = 1$ is set to $\frac{e^2}{\kappa r_{ij}} = 1$ and is con-

sidered to be the strongest interaction energy. The same scaling applies to the impurity disorder energies. The system is set to have periodic boundary conditions to avoid electrons to jump off the lattice. To prevent self-interactions a long range interaction cutoff is set to $0.5L$. Since the tunneling probability decays exponentially with the jumping length (2.13), we forbid very long, improbable jumps by setting the maximum jump length to 15 length units. The electric field is directed from left to right along the x-axis $\vec{E} = E\vec{x}$.

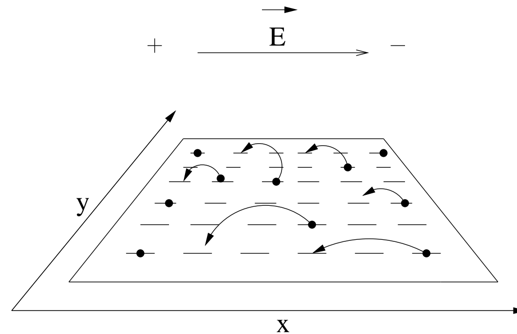

Figure 3.6: A zoom in on the model of a square lattice with $L \times L$ impurities and $0.5 \cdot (L \times L)$ mobile carriers in the presence of an electric field $\vec{E}$.

The net current is in the negative x-direction. In the electron transport only single electron jumps are allowed. This is illustrated in figure 3.6.

We wish to investigate this system in the presence of an electric field, in the temperature range where the variable range hopping occurs and when the Coulomb interactions are taken into account, that is when there is a Coulomb gap in the electronic density of states.

3.2 The Dynamic Algorithm

We use object oriented programming to code our model in C_{++}. The programme starts by initializing the system with a random electron and site energy configuration. The interaction energy of every site in the lattice is then calculated according to (3.2), summed up and stored as the total initial energy of the system.

Simulation of the electron transport is based on the theory of single electron transition rate Γ_{ij}, mentioned in section 2.1. In equation (3.5) γ_{ij}^0 represents

thermally activated electron phonon interaction. C_1 and C_2 in γ_{ij}^0 are constants, see **Appendix A** for details. $N(\Delta E_{i\to j})$ is the phonon probability distribution function - Planck distribution. n_i, n_j are site occupation numbers; $n_i = 0$ if a site i is empty and $n_i = 1$ if a site i is occupied. A jump is performed from site i to site j.

$$\begin{aligned} \Gamma_{ij} &= \gamma_{ij}^0 \, e^{-\left(\frac{2r_{ij}}{a}\right)} \, N(\Delta E_{i\to j}) \, n_i(1-n_j) \\ \gamma_{ij}^0 &= C_1 \, r_{ij}^2 \, \Delta E_{i\to j} \left[1 + \left(C_2 \cdot \Delta E_{i\to j} \right)^2 \right]^{-4} \end{aligned} \tag{3.5}$$

$$C_1 = \frac{E_1^2}{\pi \rho_0 s^5 \hbar^4} \cdot \left(\frac{2e^2}{3\kappa a} \right)^2 \qquad C_2 = \frac{a}{2\hbar s}$$

To improve the computational efficiency we implement the dynamic algorithm suggested by Tsigankov et.al [11]. The transition rate in (3.5) can be written as a product of two rates; the tunneling rate Γ^T and the activation rate Γ^A:

$$\Gamma_{ij} = \Gamma_{ij}^T \Gamma_{ij}^A = e^{-(2r_{ij}/a)} \Gamma_{ij}^A \tag{3.6}$$

The benefit of separating the original transition rate is; it saves some computational time as the tunneling rate has to be calculated only once and stored. The usage of the lattice model saves some computational memory. Because of the lattice symmetry and periodic boundary conditions the set of all possible, relative jump lengths between a site i and all other sites will be equal for every lattice site.

The choice of the activation rate Γ^A:

The activation rate must, contrary to the tunneling rate, be calculated every time a jump attempt occurs. For computational purposes we modify the expression of γ_{ij}^0 in the original transition rate (3.5). We assume that the expression $[\ 1 + (C_2(\varepsilon_j - \varepsilon_i))^2\ ]^{-4}$ in (3.5) is close to 1 and that the $r_{ij}^2 \approx \bar{r}^2$. By keeping the $\Delta E_{i\to j}$ the divergent behavior of the Planck distribution

$$N(\Delta E_{i\to j}) = \frac{1}{e^{(\Delta E_{i\to j})/kT} - 1} \tag{3.7}$$

is avoided in occasions when $\varepsilon_i = \varepsilon_j$.

The activation rate used in our simulations is then given by

$$\Gamma_{ij}^{A} = \frac{|\Delta E_{i\to j}|}{t_0} f(\Delta E_{i\to j}) n_i (1 - n_j) \tag{3.8}$$

Where $\frac{1}{t_0} = C_1 \bar{r}^2$ is set to $\frac{1}{t_0} = 1$ and defines our time scale. $f(\Delta E_{i\to j})$ is a probability distribution function of the Monte Carlo (MC) algorithm, which depends on whether the system has absorbed or emitted energy.

$$\begin{aligned} \Delta E_{i\to j} > 0 \quad &\rightarrow \quad f(\Delta E_{i\to j}) = \frac{1}{e^{\Delta E_{i\to j}/kT} - 1} \\ \Delta E_{i\to j} < 0 \quad &\rightarrow \quad f(\Delta E_{i\to j}) = \frac{1}{e^{|\Delta E_{i\to j}|/kT} - 1} + 1 \end{aligned} \tag{3.9}$$

If $\Delta E_{i\to j} > 0$, the lattice system absorbs a phonon from the phonon bath

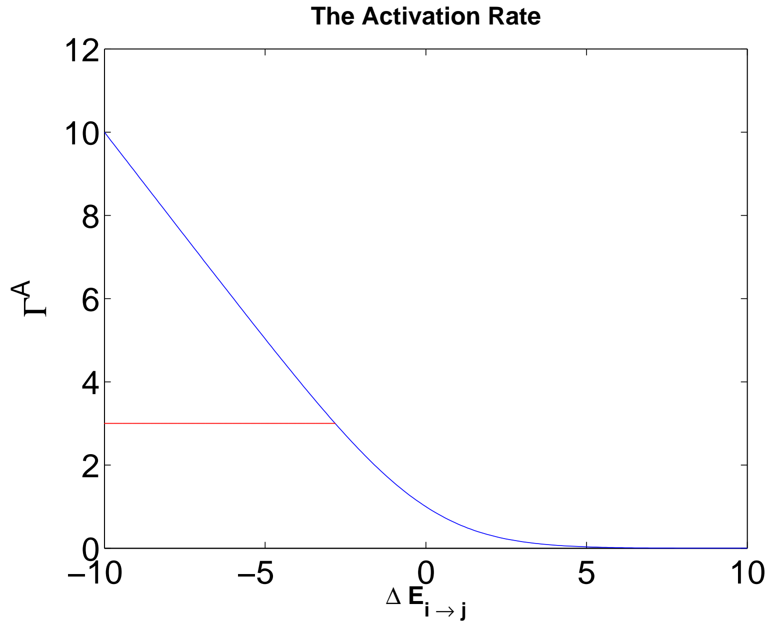

Figure 3.7: The activation rate function in the Metropolis Algorithm. The horizontal line represents the cut in the activation rate.

with an energy given by the Planck probability distribution function. If

$\Delta E_{i \to j} < 0$, the system emits a phonon into the phonon bath. We assume the phonon reservoir to be big compared to the system size. This implies that the temperature of the phonon bath is not affected by the emitted phonons.

Figure 3.7 shows our activation rate. The vertical line is a cut-off parameter P_m for Γ^A. This cut sets the lower limit ΔE_{min} for the change in the energy of a jump. The probability of a jump being accepted is given by

$$P_{acc} = \frac{\Gamma_{ij}^A}{P_m}. \tag{3.10}$$

If the energy change is smaller than ΔE_{min}, $\Gamma_{ij}^A \equiv P_m$ and the jump will definitely be accepted: $P_{acc} = 1$.

In the literature the part of Γ^A when phonon emission occurs, $\Delta E_{i \to j} < 0$, is chosen in different ways [12], [13]. We discovered that our choice of Γ^A for $\Delta E_{i \to j} < 0$ and its cut P_m strongly influences system's conductivity. This behaviour is discussed in more detail in chapter 5.

The Kinetic Monte Carlo Method - Step by Step

The programme uses a modified version of the Metropolis algorithm and executes in several steps:

1) **Initialization of the programme:**

   The programme starts with throwing out electrons at random onto a square lattice with $(L \times L)$ sites. The number of electrons is half the number of sites. Every electron possesses a random single particle energy in the interval $U_i \in [-1, 1]$. The total system energy is then calculated from to the system Hamiltonian (3.2) with no electric field present. Further all possible jumping distances r_{ij} and Γ^T are calculated and stored for later use in the jumping process.

2) **Suggestion of a single electron jump:**

   A loop of a particular number of requested jumps begins. An inner loop starts the MC algorithm: The programme picks a random site i from a uniform distribution, checks if it is filled with an electron and uses the Γ^T (3.6) to perform a random, but weighted suggestion of a site j to jump to.

3) **Change in the energy of the system:**

The change in energy the suggested jump from i to j would cause is calculated:
$\Delta E_{i \to j} = \varepsilon_j - \varepsilon_i - \frac{1}{r_{ij}} + \vec{r_{ij}} \cdot \vec{E}$

4) **Acceptance or rejection of a jump:**

Acceptance or rejection of the jump with the energy change $\Delta E_{i \to j}$ is weighted by the probability P_{acc} (3.10).

If the transition is rejected, the programme keeps account of the rejection, ends the current MC cycle and returns to the point 2) where a new MC cycle begins by randomly picking a new site i to jump from and a weighted site j to jump to. All subsequent steps are repeated.

If the energy change is accepted, the jump is performed by an update in the occupation numbers of site i and j. There is also an update in all single particle energies of the sites in the new electron configuration. The total energy of the system is calculated $E_{new} = E_{old} + \Delta E_{i \to j}$ and stored together with other information like the the jump coordinates, number of jump attempts N_{MCs}, time duration of the jump, the energy change etc.

5) **Completion of the programme run:**

As long as the requested number of jumps is not completed, after an accepted jump the programme goes back to point 2). If all jumps are executed, the programme writes the stored information of the dynamics to file and comes to an end.

3.2.1 The Monte Carlo cycle and the duration of a jump in real time.

A Monte Carlo cycle in our model is constant in time. It begins with the search of site i in point 2) and ends with a rejected or accepted jump in point 4). As already mentioned, there is a parameter N_{MCs} which counts how many jump tryouts have been made before a jump is accepted. The more improbable jumps are suggested, the more jump attempts (MC cycles) are made, and the longer time it takes to actually perform a jump. The

account of the N_{MCs} for each jump is later translated into real time by the formula

$$t = N_{MCs} \cdot t_{MC} \tag{3.11}$$

Where t_{MC} is the time of one Monte Carlo cycle and is given by

$$t_{MC} = \frac{1}{L^2 K P_m \sum\limits_{i \neq j} \Gamma_{ij}^T} \quad . \tag{3.12}$$

L is the lattice size, K is the semiconductor compensation factor and P_m is the cut-off limit for Γ^A. The expression (3.12) is a result of the development of 3 rate calculating algorithms discussed in [11]. Below these algorithms and the derivation of (3.12) will be shortly explained.

Algorithm 1:

In the first algorithm every Monte Carlo cycle results in a successful jump, and the cycle is not constant in time. A precalculation of all possible jumping rates is performed. From the total jumping rate an estimate of the physical time for a successful jump in the system is given.

Consider now the semiconductor system where Γ_{ij} is the jumping rate between two fixed points i and j. In real life jumps can occur simultaneously and the transition rate between any 2 points in the system is

$$\Gamma_{tot} = \sum_{ij} \Gamma_{ij} \tag{3.13}$$

and probability of a jump between points i and j is

$$P_{ij} = \frac{\Gamma_{ij}}{\sum\limits_{ij} \Gamma_{ij}} \quad . \tag{3.14}$$

The physical time for a jump between any two points is then

$$t_{jump} = \frac{1}{\sum\limits_{ij} \Gamma_{ij}} \tag{3.15}$$

Algorithm 2:

In the second algorithm each Monte Carlo cycle is constant in time, and every successful jump will have an individual number of cycles. The jumping

rate Γ_{ij} is calculated for each jump. An estimate of the time t_{MC} for one MC cycle is given by the jumping rate Γ_{ij}.

We look at the normalized transition rate $0 < \Gamma_{ij} < 1$ and assume that one successful jump can have many jump attempts - many MC cycles. The probability of a successful jump is then given by

$$P_{jump} = \sum_{ij} \frac{1}{N_{tr}} \; \Gamma_{ij} \tag{3.16}$$

Where N_{tr} is the number of all possible transitions and $\frac{1}{N_{tr}}$ is the probability of choosing a transition. Γ_{ij} represents the probability of a jump from i to j. The number of jump attempts resulting in one successful jump is given by

$$\frac{1}{P_{jump}} = \frac{N_{tr}}{\sum\limits_{ij} \Gamma_{ij}} \tag{3.17}$$

Every jump attempt takes the time t_{MC}, so the time of one successful jump, with inserting the result from (3.15), is now

$$t_{jump} = \frac{1}{\sum\limits_{ij} \Gamma_{ij}} = \frac{1}{P_{jump}} \cdot t_{MC} = \frac{N_{tr}}{\sum\limits_{ij} \Gamma_{ij}} \cdot t_{MC} \tag{3.18}$$

Rearranging with respect to t_{MC} we get

$$t_{MC} = \frac{1}{N_{tr}} \quad . \tag{3.19}$$

Algorithm 3:

The last algorithm is the one we use, described in section 3.2. The estimate of t_{MC} is done for a separated rate $\Gamma_{ij} = \Gamma^T_{ij} \cdot \Gamma^A_{ij}$. The jump suggestions are weighted by the precalculated transition rates $\Gamma^T_{tot} = \sum\limits_{ij} \Gamma^T_{ij}$. The acceptance of the jump is governed by Γ^A_{ij} which is calculated for each jump.

The probability of choosing a transition pair ij is

$$P^T_{ij} = \frac{\Gamma^T_{ij}}{\sum\limits_{ij} \Gamma^T_{ij}}$$

and the probability of accepting this transition is

$$P_{ij}^{A} = \frac{\Gamma_{ij}^{A}}{P_m} \quad . \tag{3.20}$$

The probability of making a successful jump is given by

$$P_{jump} = \sum_{ij} \frac{\Gamma_{ij}^{T}}{\sum_{ij} \Gamma_{ij}^{T}} \cdot \frac{\Gamma_{ij}^{A}}{P_m} = \frac{1}{P_m} \frac{\sum_{ij} \Gamma_{ij}}{\sum_{ij} \Gamma_{ij}^{T}} \tag{3.21}$$

The number of jump attempts resulting in one successful jump is again

$$\frac{1}{P_{jump}} = \frac{P_m \sum_{ij} \Gamma_{ij}^{T}}{\sum_{ij} \Gamma_{ij}}$$

Following the procedure in equation (3.18) the time of one jump is

$$t_{jump} = \frac{P_m \sum_{ij} \Gamma_{ij}^{T}}{\sum_{ij} \Gamma_{ij}} \cdot t_{MC} = \frac{1}{\sum_{ij} \Gamma_{ij}} \tag{3.22}$$

which gives

$$t_{MC} = \frac{1}{P_m \sum_{ij} \Gamma_{ij}^{T}} = \frac{1}{P_m \sum_{i} \sum_{i \neq j} \Gamma_{ij}^{T}} \tag{3.23}$$

For a lattice system the term $\sum_{i \neq j} \Gamma_{ij}^{T}$ is independent on i, so

$$P_m \sum_{i} \sum_{i \neq j} \Gamma_{ij}^{T} = P_m L^2 \sum_{i \neq j} \Gamma_{ij}^{T} \quad .$$

The programme always chooses the i coordinate from the occupied sites, which reduces L^2 to $L^2 K$. The time for one MC cycle is therefore given by

$$t_{MC} = \frac{1}{L^2 K P_m \sum_{i \neq j} \Gamma_{ij}^{T}} \quad .$$

Chapter 4

Ohmic Conductivity

4.1 System under influence of an electric field

We now investigate our system under influence of an electric field $\vec{E}$. In order to do so it is necessary to know whether parameters like the electric field itself, the temperature T and the size of the lattice L are correctly chosen for the further calculations. Another aim is to check if our simulation programme works properly and is able to reproduce the previously derived law of Efros and Shklovskii (2.35), which states that the electric conductivity behaves as

$$\sigma = \sigma_0 \exp\left[-\left(\frac{T_0}{T}\right)^p\right] \ , \ p = \frac{1}{2} \tag{4.1}$$

in the presence of Coulomb interactions. In order to systemize our approach we start with finding which field strength gives an Ohmic conductivity behaviour at different temperatures. Next we investigate how the conductance varies with system's size at fixed temperature and electric field. Last but not least we use a convenient system size to calculate the conductivity at different temperatures using a proper field and compare our results to (4.1).

4.2 Electric field strength

We choose a temperature range $T \in [0.02,\ 0.5]$ where we expect to find the conductivity behaving as described by (4.1). The lower limit of the interval is set from results of Martin Kirkengen's work [14]. T=0.02 is the lowest temperature at which our system tends to an equilibrium during the simulation time. The upper temperature limit is set by the disappearance of the Coulomb gap. The first aim is to find a field strength at which the system

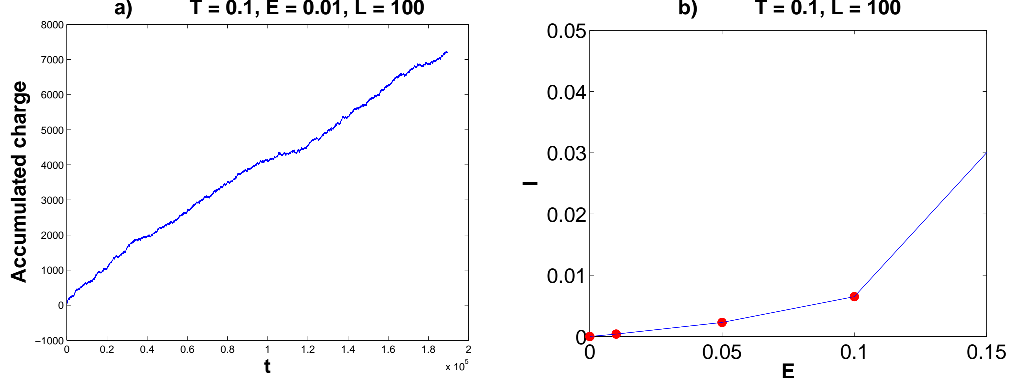

Figure 4.1: a) Accumulated charge as function of time under influence of $\vec{E}$.
b) Current versus electric field $\vec{E}$. The points are extrapolated to origo.

shows Ohmic behaviour at different temperatures. We start with investigating the system for $T = 0.1$ and L=100. Our programme was run for 10^6 jumps at following fields: $E = [0.01,\ 0.05,\ 0.1,\ 0.5,\ 1.0]$. Each run produced accumulated charge versus time graph similar to figure 4.1a. The accumulated charge can be considered as a kind of dipole moment. Our system is set to have periodic boundary conditions, therefore the dipole moment we refer to is not the same as the exact definition:

$$p = \sum_i q_i r_i$$

where p is the dipole moment, r_i is the distance from the origin to a given site i and q_i is the charge of the site i. In the accumulated charge versus time graphs we use the linear part of the sequence to calculate the slope $\frac{dp}{dt}$. The linear part indicates that the system has reached a stationary state at a given field. The slope is obtained by linear fitting and enables us to calculate the 2D current and current density by a simple scaling:

$$j = \frac{Q}{tL} = \frac{1}{L^2} \cdot \frac{dp}{dt} \tag{4.2}$$

where Q is the total charge, $j = \frac{Q}{tL}$ is the 2D current density and the second $\frac{1}{L}$ is from the total length the electrons must travel in order to contribute to the transport. The current of the 2D system is then given by

$$I = jL = \frac{1}{L} \cdot \frac{dp}{dt} \tag{4.3}$$

As seen from figure 4.1a, for sufficiently high temperatures and appropriate fields the relation between the accumulated charge and time is very close to linear. From Ohm's law $V = RI$ and the relation between the voltage and the electric field $V = EL$ we see that since $j = \sigma E$ and the 2D conductivity is $\frac{1}{R}$, we have the relation

$$j = \frac{I}{L} = \frac{1}{R} \cdot E = \sigma E$$

It is therefore possible to plot the corresponding current and field values and seek the linear part of the slope, which indicates ohmic system behaviour with a constant conductivity which implies a constant resistance. Finally we read off the field strength of the ohmic range. As seen from figure 4.1b for $T = 0.1$ it looks like a field strength of $E = \frac{T}{10} = 0.01$ is in the Ohmic region when we extrapolate the lowest point to (0,0).

Similar approach is used for the lower temperatures where we followed the procedure described above. During simulations it was clear that 10^6 jumps was not enough to get a linear accumulated charge versus time dependence, the results were mostly noise. By consequence the number of jumps was increased to $\sim 10^7$. The field strengths were varied as $E = [\frac{T}{100}, \frac{T}{40}, \frac{T}{20}, \frac{T}{10}]$ where it is assumed that fields $E >> \frac{T}{10}$ quite certainly would give a current in the non-Ohmic range for the lower temperature runs. For $T = 0.02$ the accumulated charge versus time plots didn't give a visible charge transport. $T = 0.03$ and $T = 0.04$ has charge transport only for the strongest field $E = \frac{T}{10}$. Since each field strength contributes with one point to the I vs E graph, there weren't sufficient data to define an Ohmic range for $T = 0.03$ and $T = 0.04$. $T = 0.05$ is the lowest temperature for which it is possible to calculate several points for the I vs E plot from our chosen temperatures and fields. In the case of $T = 0.05$ we have 3 calculated points in the Ohmic field range and the extrapolated (0,0) point. The last and rightmost point in figure 4.2d is included to give a better picture of the contrast between the Ohmic and the non-Ohmic behaviour.

Comparing figures 4.1a and 4.2a,b,c we see that for $T = 0.05$ there are considerable fluctuations in the data. To find the current we use two methods for finding the slope $\frac{dp}{dt}$ and compare the results by two methods:

1) Linear fitting in Matlab.

2) Method of least squares for the best strait line $y = mx + c$ for a set of points.[15]

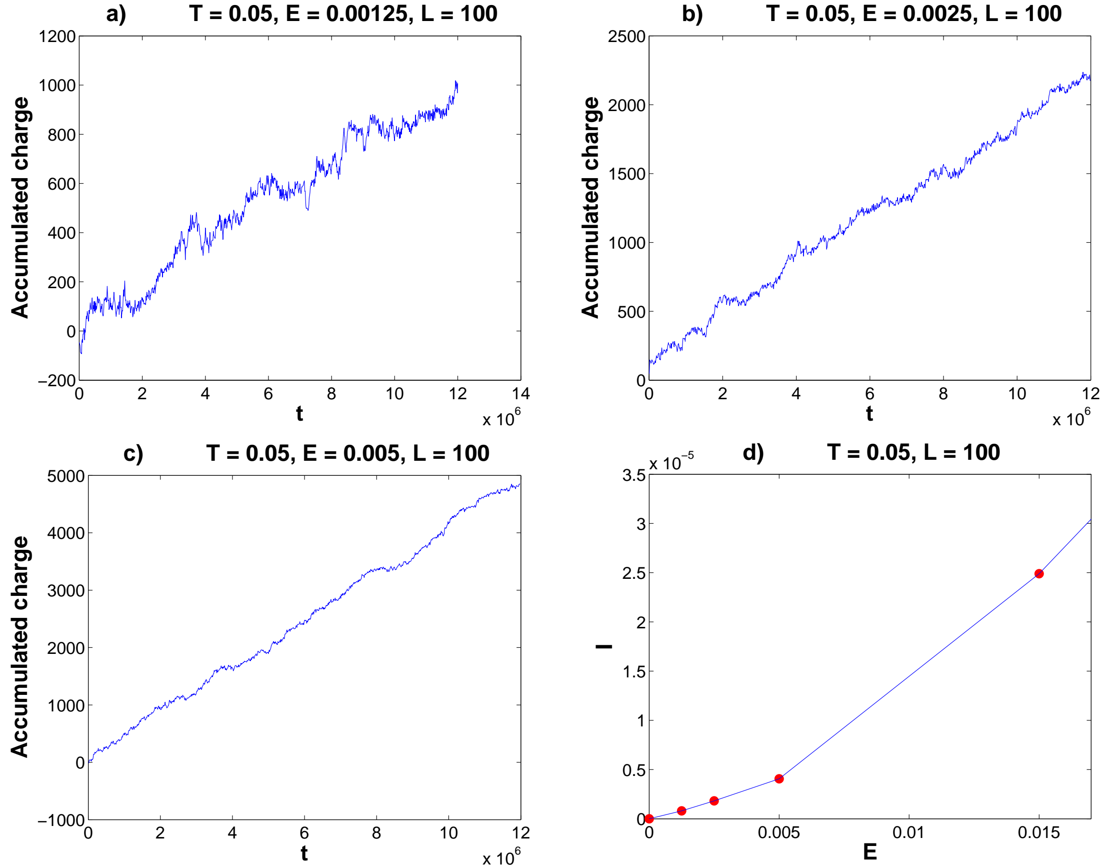

Figure 4.2: a,b,c - Accumulated charge under influence of 3 different field strengths E.
d - Current versus electric field:
The (0.0) point is extrapolated, the 3 next points are calculated from slopes of a,b,c.
The last, rightmost point is calculated in the same way with a stronger field.

Method number 2) also gives estimates of the errors dm for the given slope m and dc for the given y-intercept c. We calculate slopes for the whole set of 10^7 jumps for graphs a, b and c in figure 4.2. A comparison of the slopes from the two methods gives equal results up to the fourth decimal. The relative error $\frac{dm}{m}$ estimated by method 2) is of the order of 0.2%. From the final I vs E graph in figure 4.2d we can assume that also for $T = 0.05$ a field of $E = \frac{T}{10}$ is appropriate to give an Ohmic behaviour. From now on the field of $E = \frac{T}{10}$

is used in all further calculations for temperatures

$$T \in [0.05, 0.5] \tag{4.4}$$

in this chapter. For $T < 0.05$ we weren't able to show that $E = \frac{T}{10}$ is in the Ohmic regime due to noise. But we can suggest that also for this and lower temperatures $E = \frac{T}{10}$ is within the Ohmic range.

4.3 Conductivity and lattice size

In order to find a proper lattice size where the energy configurations don't influence the conductivity too much, we chose to run calculations for $T = 0.1$ in the Ohmic range with $E = \frac{T}{10} = 0.01$. For the lattice size the following variations were used: $L \in [10, 20, ...100]$. This was done for 10^6 jumps. For each lattice size we did 4 parallel runs with 4 different disorder energy configuration samples. The reason is to see if the difference in the energy configurations contributes to considerable fluctuations in the conductivity. For small systems we know that the site energy configurations in the lattice contribute to so-called mesoscopic fluctuations in the conductance. These fluctuations are smeared out as the system size increases and the conductivity reaches its macroscopic value. It is therefore of interest to see if the dispersion coming from different site energies decreases as the system size increases.

We expect to see a stabilization of the σ as it approaches its macroscopic value with increasing L. Our first results, the leftmost points in figure 4.3, don't at all live up to our expectations. The conductivity increases as the system size increases. We further increased the system size to - $L \in [150, 200, ...500]$ and still got no stabilization of the conductivity. The graph of figure 4.3 still grows. From the article of Tsigankov and Efros [12] we know that calculations for electric conductivity have been successfully done for a typical lattice size less than $L = 100$. The possibility that a bigger system doesn't yet reach the stationary state after 1 million jumps influenced us to increase the running time to several million jumps.

We run our system with $6 \cdot 10^6$ jumps for $L = 100$ and $3 \cdot 10^6$ for $L = [150, 200, 250, 300]$. Compared to our earlier calculations in figure 4.3, the results of figure 4.4 show a considerable stabilization of σ versus L due to

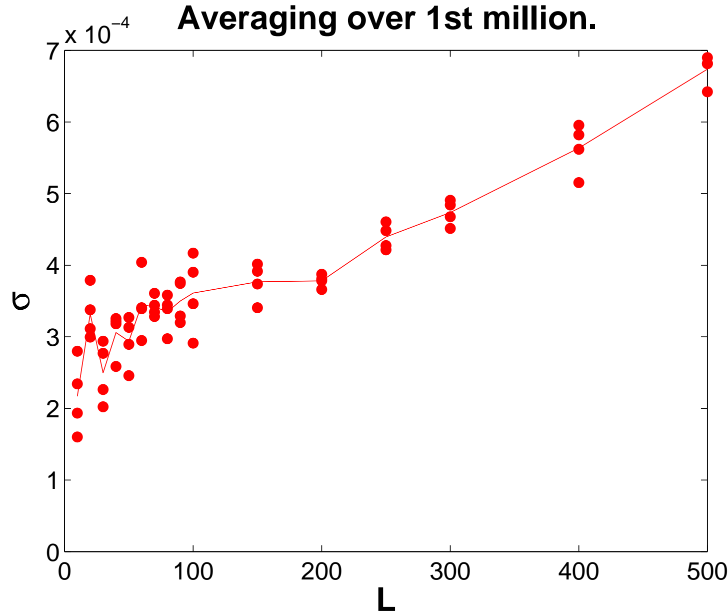

Figure 4.3: Conductivity as function of the lattice size at $T = 0.1$, $E = 0.01$. Calculations are done for a "short run" of 10^6 jumps. Continuous line is the average of the dots.

increased number of jumps. They also show that averaging over as many jumps as possible and excluding the first million gives a better result. The former is due to the fact of a better statistical results from more data. The latter is due to the already mentioned stationary state. Figure 4.5 shows a comparison of the conductivity calculated for the short runs (upper red line) and for the long runs (lower blue line) as function of the system size. It is clear that for longer time runs the conductivity stabilizes in accordance with our earlier predictions. There is no apparent reason to assume that σ will deviate much from the the blue line for bigger L as long as the system is run through enough jumps. For the smallest systems sizes we assume a spreading similar to the short run calculations. There is also a slight tendency of a decreasing seed dispersion as the system size is increased. By this we conclude that for $T = 0.1$ a lattice size of $L = 100$ is sufficient.

From the book of Efros and Shklovskii [2] we know that the correlation length of the system ℓ is inversely proportional to temperature to the power

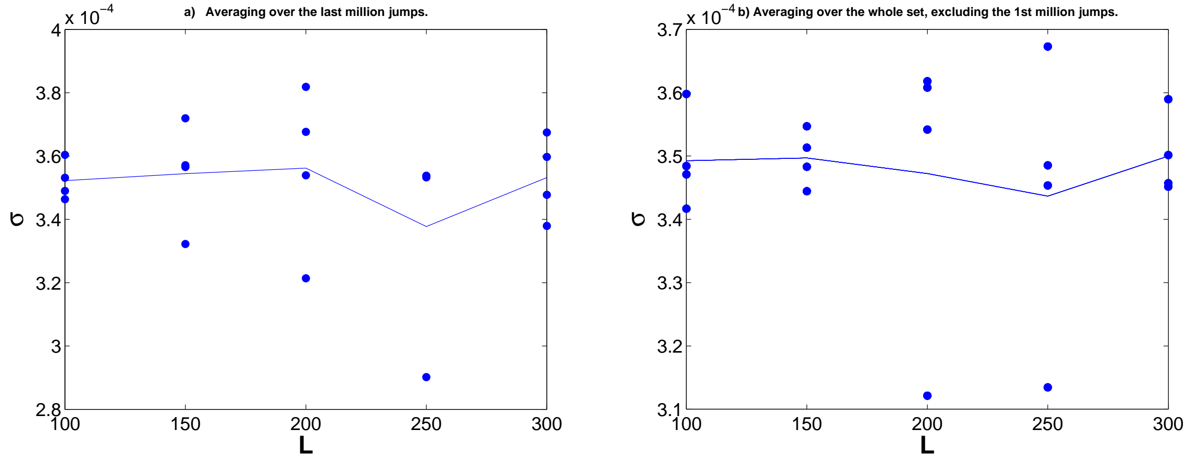

Figure 4.4: Conductivity as function of the lattice size at $T = 0.1$, $E = 0.01$. Calculations are done for longer time runs of $3 \cdot 10^6$ and $6 \cdot 10^6$ jumps. Continuous line is the average of the 4 disorder energy samples - dots.

of the critical exponent $\nu \approx 1.33$ [11]:

$$\ell \propto \frac{1}{T^{\frac{\nu}{2}}} \tag{4.5}$$

From this we know that the correlation length increases as the temperature decreases. If the correlation length is bigger than the system size, the mesoscopic fluctuations will start to influence the conductivity. We must therefore check whether $L = 100$ can be used for the lower values of our temperature interval (4.4). We do similar calculations as above for σ versus L for our lowest temperature $T = 0.05$ with long runs of 10^7 jumps. Plots in figure 4.6 resemble figures 4.3 and 4.4 in several ways. In 4.6a we get the picture of a non-stabilizing conductivity, even for 10^7 jumps. From this we can for now assume that at lower temperatures the bigger a system, the longer it must be run to achieve a stable conduction state. Previous knowledge of increasing the running time gives us the result of 4.6b. Here the points for $L = 100$ and $L = 200$ are kept from 4.6a, whereas for $L = 300$ and $L = 400$ the running time is doubled to $2 \cdot 10^7$ jumps. The development of the blue line of the figure in question is easy to recognize from the behaviour of the lower blue line in figure 4.5. It seems from this plot that for the temperature $T = 0.05$ it is okay to use a system size of $L = 300$ or $L = 200$. Even $L = 100$ can be sufficient.

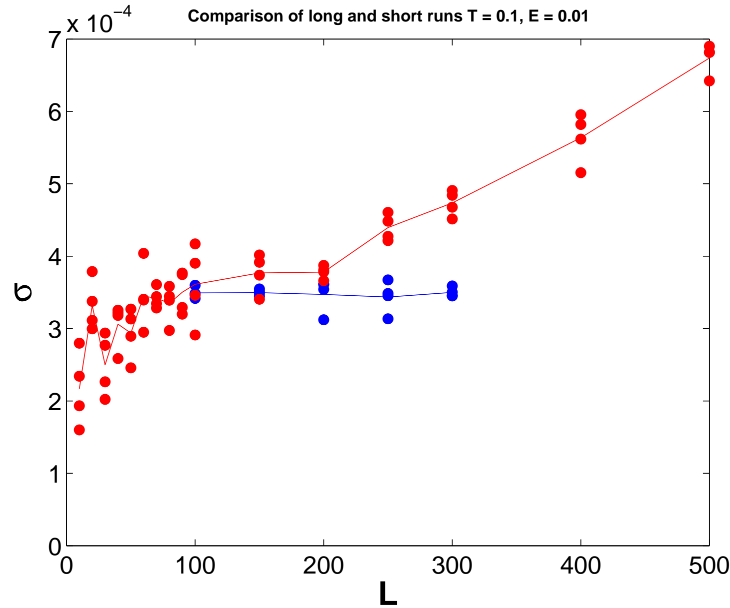

Figure 4.5: Comparison of conductivity as function of the lattice size at $T = 0.1$, $E = 0.01$ *for short runs (upper red line) and for long runs (lower blue line). Continuous lines are the sample averages.*

The final conclusion to our results is: for "high" temperatures in vicinity of $T = 0.1$ and above it, it's safe to use $L = 100$. For lower temperatures the same length can be used. But to secure a macroscopic conductivity, that our system size is bigger than the correlation length, we use $L = 200$ for the lower temperatures ($T < 0.1$) of the interval (4.4). We also see that for the lower temperatures the number of jumps it takes the system to reach a stationary state increases.

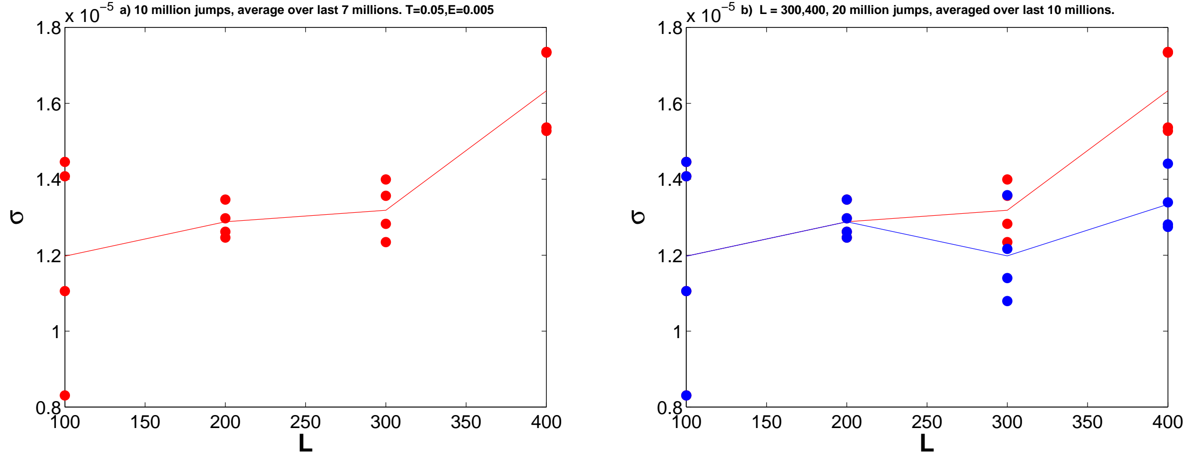

Figure 4.6: Conductivity as function of the lattice size at $T = 0.05$, $E = 0.005$.
a) Calculations are done for 10^7 jumps - red.
b) Calculations for $2 \cdot 10^7$ jumps for $L = 300$ and $L = 400$ - blue.

4.4 Confirmation of Efros-Shklovskii law

We now have enough information on the values of E and L to be able to run calculations for the electric conductivity versus temperature. From theoretical predictions of Efros and Shklovskii discussed in section 2.5 we look at the temperature range of $T \in [0.05, 0.5]$, where we expect to see the behaviour of (4.1) in our system.

From the calculations in section 4.3 on the conductivity versus lattice size for the higher temperatures $T \in [0.1, 0.5]$, we chose the lattice size of $L = 100$. For the lower temperatures $T \in [0.05, 0.09]$ we used $L = 200$. For all temperatures we ran our system with 4 samples of different energy disorder through 10^7 jumps with a field strength of $E = \frac{T}{10}$. For each temperature we went through the same procedure as described in section 4.2 and used equation (4.2) to obtain the current density. Finally the conductivity was found from the well known relation between the current density and the electric field:

$$\vec{j} = \sigma \vec{E} \tag{4.6}$$

The results can be plotted in various ways. Figure 4.7 shows the most frequent choice of axes in the Coulomb glass research area when the interactions

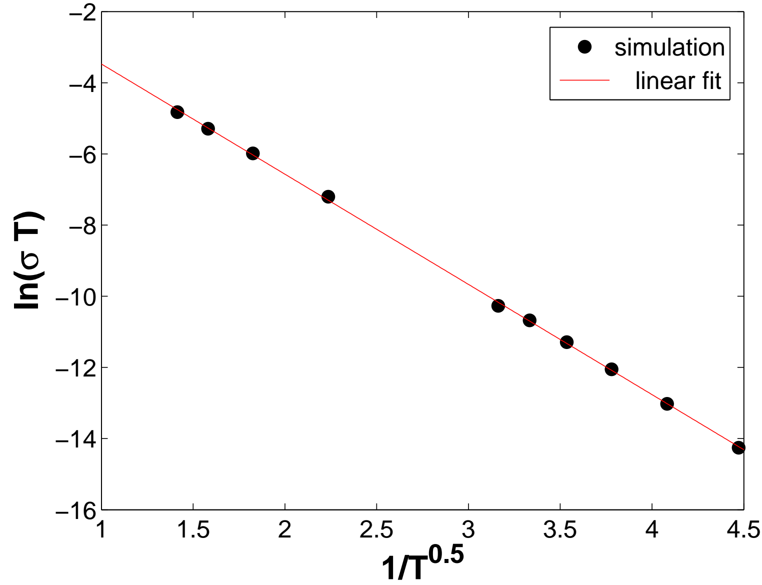

Figure 4.7: Conductivity as function of temperature plotted as $\ln(\sigma T)$ *versus* $\frac{1}{T^{0.5}}$.

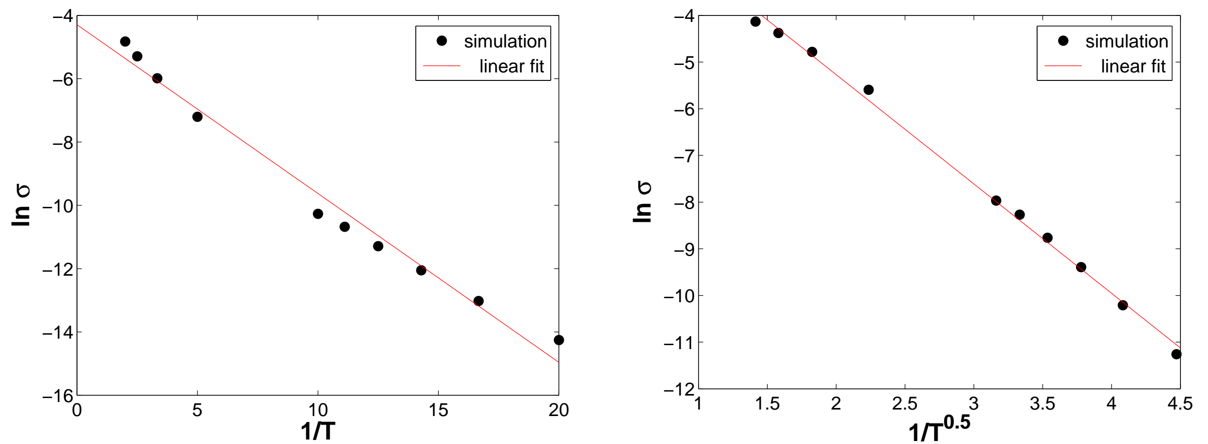

Figure 4.8: Left - conductivity as function of temperature plotted as $\ln\sigma$ *versus* $\frac{1}{T}$. *Right - conductivity as function of temperature plotted as* $\ln\sigma$ *versus* $\frac{1}{T^{0.5}}$.

are taken into account [12]. A fairly good linear fit shows that p from (4.1) is close to 0.5. The leftmost plot in figure 4.8 is included for comparison and confirmation of the points not fitting well with $p = 1$.

For many years there has been an ongoing discussion on whether the pre-exponential factor σ_0 in the conductivity (4.1) is temperature dependent or not. By comparing the results in figure 4.7 with the rightmost plot in figure 4.8, the plot in figure 4.7 shows that the results fit slightly better with a temperature dependent $\sigma_0(T) \sim \frac{1}{T}$.

We therefore focus on the plot in figure 4.7. From its data we can easily find the constant T_0 as the square of the slope from a linear fit:

$$\sigma T = Ae^{-(\frac{T_0}{T})^{\frac{1}{2}}} \quad \rightarrow \quad \ln(\sigma T) = \ln A - T_0^{\frac{1}{2}} \cdot \frac{1}{T^{\frac{1}{2}}} \tag{4.7}$$

$T_0 \approx 9.6$ with the error of $\delta T_0 \approx 0.1$. The drawback of this method lies in the assumption that $p = \frac{1}{2}$. Experiments [2] chapter 9, show that the values of p vary between $0.18 - 0.7$ in amorphous semiconductors and between $0.25 - 0.7$ in crystalline semiconductors. In both cases however, most values of p group around 0.5.

The Method of A. Ogielskii

Another suitable way of plotting the results was introduced to us by Ogielski [16]. This method gives an estimate of both T_0 and p which are found in the following way: We begin with taking the logarithm of the equation (4.1) and invert it.

$$\frac{1}{\ln \sigma} = \frac{1}{\ln A - (\frac{T_0}{T})^p}$$

Further we can multiply the above expression by $-T$ and approximate it for small T, when the constant $\ln A$ in the denominator is negligible, by

$$\frac{-T}{\ln \sigma} \approx T_0^{-p} \cdot T^{(p+1)}$$

By taking yet another logarithm we end up with a straight line where the slope is given by $(p + 1)$ and the y-intercept is given by $-p \ln T_0$.

$$\ln(\frac{-T}{\ln \sigma}) \approx (p + 1) \ln T - p \ln T_0 \tag{4.8}$$

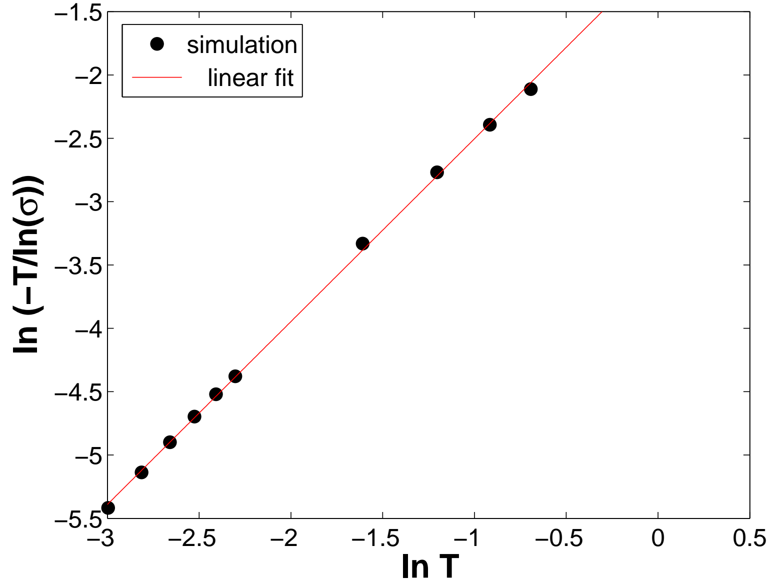

Figure 4.9: Conductivity as function of temperature plotted by the method of Ogielski.

A linear fit on the points in figure 4.9 gives us $T_0 \approx 10.9$ with an error of $\delta T_0 \approx 0.07$ and $p \approx 0.44$ with an error of $\delta p \approx 0.01$.

It seems that the way of plotting the data with the method of Ogielski give somewhat different results compared to the method in figure 4.7. One reason might be the approximation of setting $\ln A \approx 0$. In addition, the reliability of the plot in figure 4.9 is weakened by not including data which stretch over a wide enough range of temperatures. In a logarithmic plot it is usually preferred that the exponent variations are of the order of 3. In our case it is approximately of the order of 2. Unfortunately we cannot include calculations for lower temperatures, as there are difficulties in obtaining a stable current. Nor can we increase the temperature, as the variable range hopping is predicted to cease and the Coulomb gap smears out.

Figure 4.10 shows the Coulomb gap in our system's density of states for the lowest and highest temperatures of the chosen temperature interval; $T = 0.05$ and $T = 0.5$. The taller graph is for the lowest temperature $T = 0.05$, and the lower graph is for the highest $T = 0.5$. The leftmost "hill" of each graph

represents the occupied states and the rightmost "hill" represents the empty states. The Coulomb gap and its smearing with increasing temperature is clearly observed.

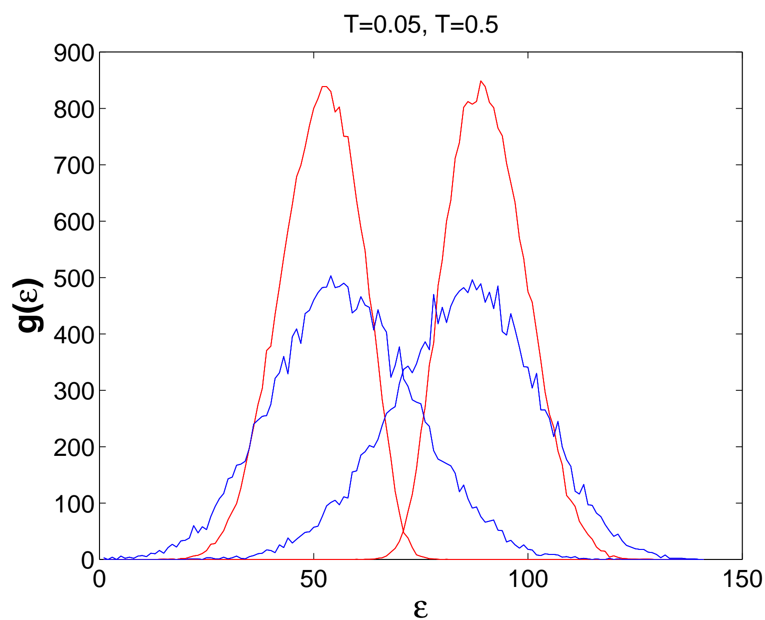

Figure 4.10: The Coulomb gap in the density of states for $T = 0.05$ - the tall graph, and for $T = 0.5$ - the low graph. The smearing of the gap with increasing temperature is observed.

4.4.1 Numerical precision of the p-exponent.

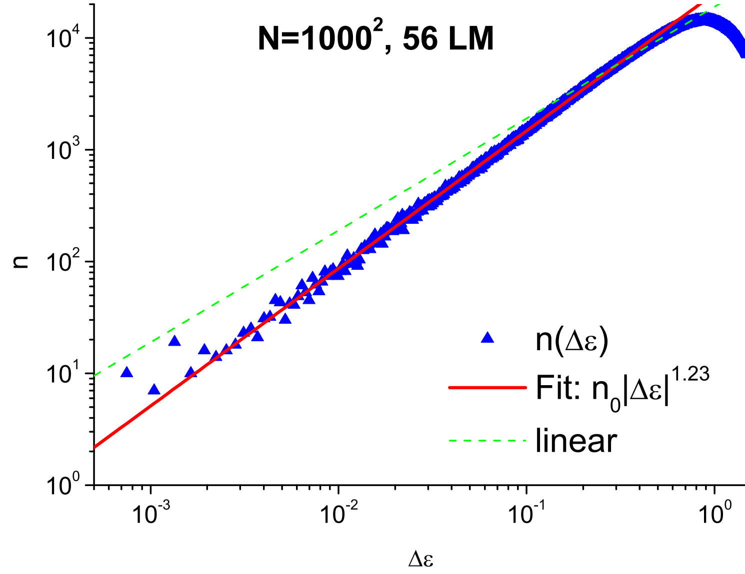

Figure 4.11: Earlier 2D calculations of the density of states versus energy done on our system. The shape of the gap is linear with the slope of 1.23 *which is close to the value of* 1 *predicted by Efros & Shklovskii. As the* $\Delta\varepsilon$ *approaches zero the gap is smeared out due to non-zero temperature [17].*

As already mentioned in the beginning of section 4.4 and in section 2.5, the studies on the conductivity in semiconductors show that the exponent p varies with the type of semiconductor and is directly dependent on the shape of the density of states near the Fermi level μ.

In section 2.5 the dependence of p on the density of states $g \propto |\varepsilon - \mu|^n$ is shown to be given by

$$p = \frac{n+1}{n+d+1} \ . \tag{4.9}$$

Calculations from earlier research done on our 2D-system represented in figure 4.11, show that the numerical value of the exponent of the density of states is $n = 1.23$ [17]. The ideal value, which gives $p = \frac{1}{2}$ in 2 dimensions,

is $n = 1$. We therefore want to compare the value of $p = 0.44$ achieved from figure 4.9 to the value of p given by a relation in equation (4.9) with $n = 1.23$.

Inserting $n = 1.23, \quad d = 2$ into equation (4.9) leads to $p = 0.53$.

Chapter 5

Non-Ohmic Conductivity

Now that we are aware of the proper parameters of the temperature interval where the variable range hopping occurs, the proper lattice size and an approximate Ohmic field limit, we are interested in investigating our system in the non Ohmic field range - $E > \frac{T}{10}$.

From the experimental work of Aronzon et.al [8], there is a reason to believe that the non-Ohmic conductivity has a field dependency of

$$\sigma(E,T) = \sigma_0 \; exp \left(\alpha \frac{E^{1/2}}{T} \right) \quad \alpha = constant. \tag{5.1}$$

We therefore choose our field values in terms of $E = T^2$.

The program is run with following parameters:

$$E = T^2 [\frac{1}{4}, \frac{1}{2}, 1, 2, 4, 6, 9, 12, 16, 20, 25]$$

with

$$T \in [0.05, \; 0.5] \; .$$

For better statistics we start with 8 different disorder energy samples. The number of jumps is chosen to be 20 million for $T \in [0.05, 0.09]$ with $L = 200$, and 10 million jumps for $T \in [0.1, 0.5]$ with $L = 100$. Figures 5.1 and 5.2 show the results represented by temperatures $T = 0.09$, $T = 0.2$ and $T = 0.5$. The conductivity first increases monotonically with the field, reaches a maximum value, after which it decreases. As the conductivity decreases the current density $j = \sigma/E$ reaches a stable value.

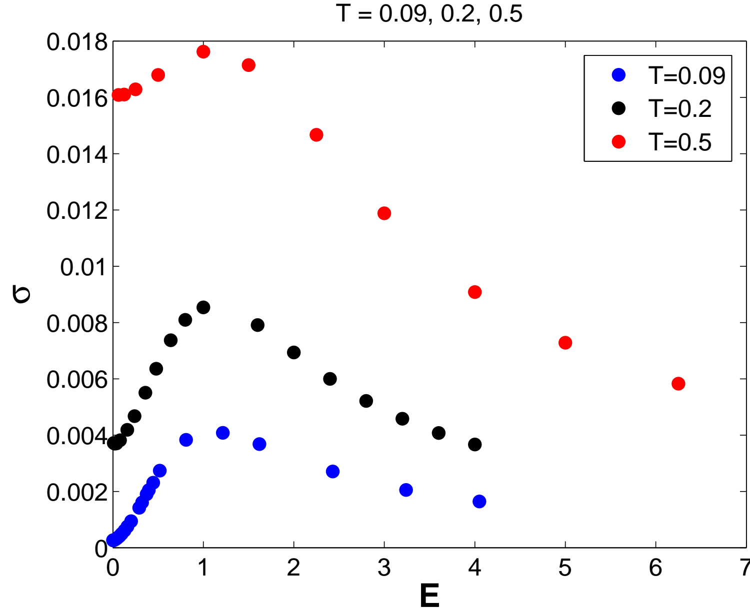

Figure 5.1: Conductivity σ versus the non-Ohmic electric field strength E.

We want to understand why the decreasing conductivity behaviour occurs. We try to increase the system size in order to check if the decrease is due to lattice size effect. This is done for $T = 0.5$ and $L = 200$. We also increase the field strength $E = T^2[100, 150, 200, 300, 400, 500]$ for the lowest temperatures to check if the decreasing behaviour of the conductivity could occur due to temperature effects. The results show no difference.

We suspect the decrease in σ to be influenced by the choice of the cutoff parameter P_m in Γ^A (3.8) in the dynamic algorithm. The cutoff is set to $P_m = 3$ by default. We run our system as the cutoff is increased: $P_m = [20, 50]$ at $T = 0.2$. The results are shown in figures 5.3 and 5.4. As the P_m is increased the conductivity graph in figure 5.3 preserves its shape, but reaches the maximum and decreases at higher field strengths. Correspondingly the current density in figure 5.4 seems to stabilize at higher field values when the conductivity begins to decrease.

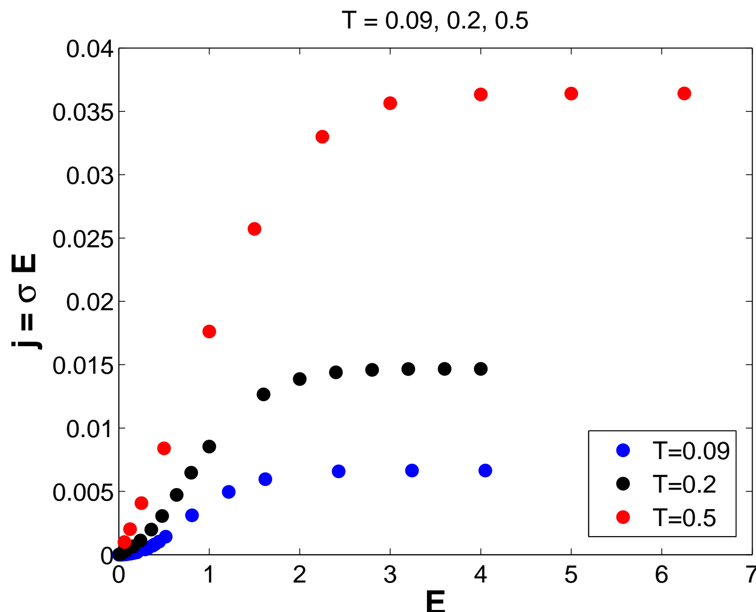

Figure 5.2: Current density $j = \sigma E$ corresponding to σ in figure 5.1.

The influence of the P_m parameter on the conductivity:

In the dynamic algorithm in section 3.2, the P_m parameter influences the acceptance of a suggested jump. To every P_m value there is a corresponding value of the system's energy change $\Delta E(P_m)_{i\to j} = \Delta E_{min}$. In the Metropolis algorithm the following happens: If the $\Delta E_{i\to j}$ of a particular jump is smaller than the ΔE_{min}, the jump will always be accepted. This means that if our cutoff limit P_m is small and the electric field is strong, the electrons will jump against the field to decrease their potential energy. Most jumping suggestions will have $\Delta E_{i\to j} < \Delta E_{min}$ because of the dominating last term in

$$\Delta E_{i\to j} = \varepsilon_j - \varepsilon_i - \frac{1}{r_{ij}} + \vec{r_{ij}} \cdot \vec{E} \quad .$$

Hence all the jumps with $\Delta E_{i\to j} < \Delta E_{min}$ will be accepted with the probability of 1.

Variable Range Hopping will be defeated by nearest neighbour hopping with $r_{ij} = 1$, since these are the most probable and frequent jumping suggestions weighted by $\Gamma_{ij}^T = e^{-2r_{ij}/a}$. More of the jumps are easily accepted the stronger

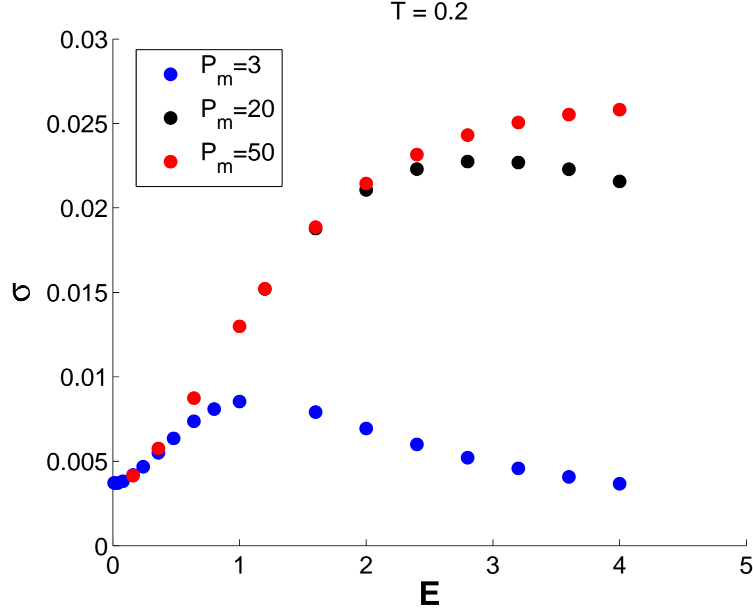

Figure 5.3: The conductivity behaviour as the cut-off parameter P_m is varied.

the field and the lower the P_m is. The acceptance of nearest neighbor jumps stabilizes the current. From the relation

$$\vec{j} = \sigma \vec{E} \tag{5.2}$$

we directly see that to get a stable current as the electric field is increased, the conductivity must decrease. This is the explanation of the decreasing conductivity behaviour in figure 5.1.

Discussion on the correct use of the cutoff phonon frequency.

Because of the phonon assisted tunneling we should give a greater thought to the physical meaning of the cut-off parameter P_m. The phonons cannot have an infinitely large frequency ω and every lattice has an upper phonon frequency limit. The vibrational modes cannot have wavelengths shorter than two times the lattice constant: $\lambda_{min} = 2\ell$. The largest possible phonon oscillation frequency is then $f_{max} = \frac{s}{2\ell}$ where s is the speed of sound in the material and ℓ is the lattice constant.

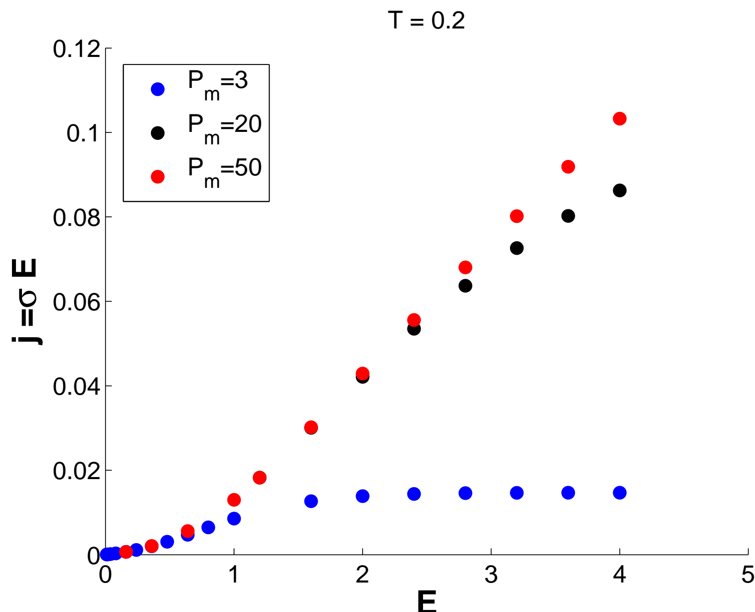

Figure 5.4: Current density $j = \sigma E$ corresponding to σ in figure 5.3 as the cut-off parameter P_m is varied.

This means that the largest possible quantized phonon energy is given by $E_{max} = \hbar\omega_{max} = hf_{max} = \frac{hs}{2\ell}$. The phonon modes are grouped into high frequency optical modes and low frequency acoustic modes which can both be either longitudinal or transverse [18]. These have different dispersion relations - the phonon frequency ω as a function of the phonon wave vector q.

At low temperature the optical modes are frozen out and the lattice vibrations are governed by the acoustic modes. In the Miller and Abrahams model the hopping rate is a direct result of the assumption of only one acoustic branch being active at low temperatures and the dispersion relation is assumed to be linear. However, a multiphonon interaction and creation of optical phonons by the electric field cannot be excluded.

This means that the biggest phonon interaction energy corresponding to the $|\Delta E_{min}|$ of some given P_m parameter in our model should be

$$|\Delta E_{min}| \leq \frac{hs}{2\ell} \quad .$$

Also, the cut in the Γ^A should probably be vertical instead of horizontal, as illustrated in figure 5.5. By this the generality of the numerical model can be connected to explicit solids where the P_m can be adjusted in accordance with the lattice constant of the material in question.

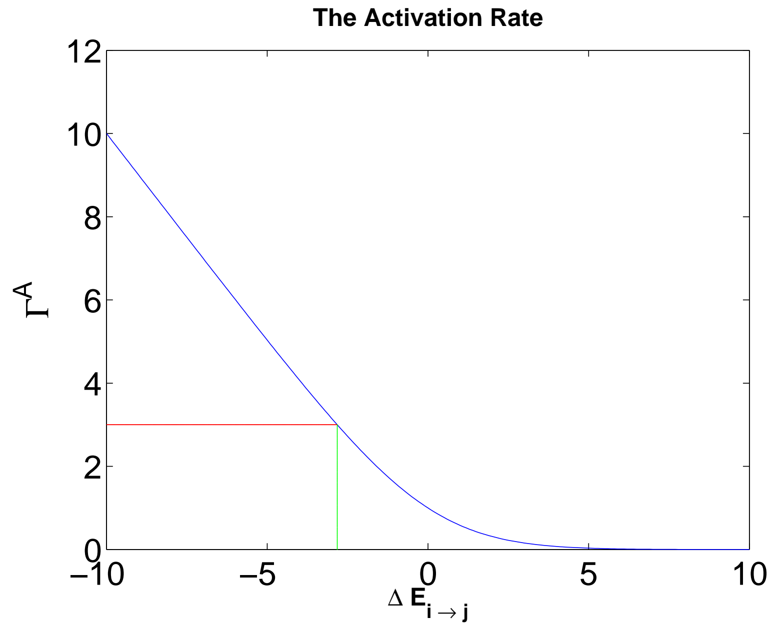

Figure 5.5: The horizontal cut is currently used in the Metropolis algorithm in our simulation programme. The vertical cut in Γ^A can be used to set an upper limit to the phonon interaction energy.

Comparison of the simulation data with the experiments by Aronzon et al.

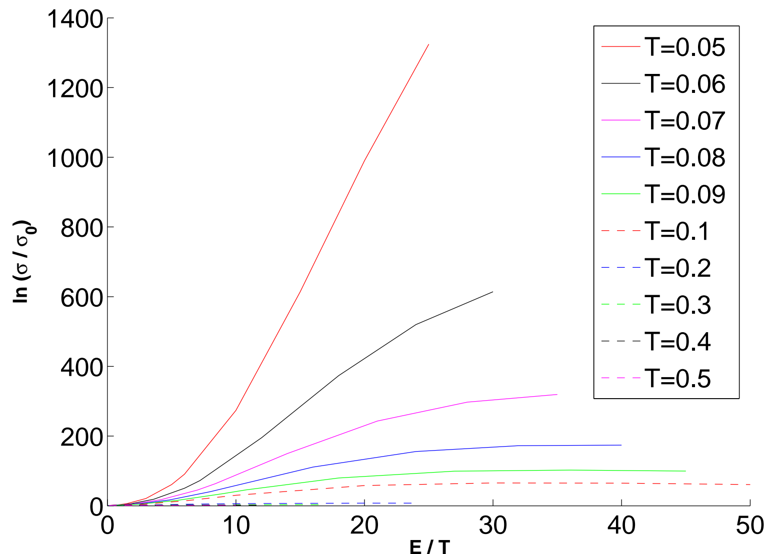

Figure 5.6: Simulation data: the logarithm of the conductivity σ as a function of E/T at temperatures $T \in [0.05, \quad 0.5]$ and $P_m = 50$. σ_0 is the Ohmic conductance.

In section 2.6 we mentioned the results of Aronzon et al. on the conductivity in the non-Ohmic field region. Here we present the results of our simulations. Figure 5.6 shows a $\frac{E}{T}$ collapse plot of our data with $P_m = 50$ similar to figure 2.12. Figure 5.7 shows a $\frac{E^{1/2}}{T}$ collapse plot with $P_m = 50$ similar to figure 2.13. Figure 5.8 shows a $\frac{E}{T^2}$ collapse plot with $P_m = 50$. The spreading of the collapsed curves at high field strengths are due to the P_m cutoff.

In resemblance with the experimental results of Aronzon et al. we observe that our data fit the $ln(\sigma/\sigma_0) \propto E^{1/2}/T$ relation better than the $ln(\sigma/\sigma_0) \propto E/T$. But from the comparison of the plots in figure 5.7 and 5.8 it is difficult to determine whether $ln(\sigma/\sigma_0) \propto E^{1/2}/T$ or $ln(\sigma/\sigma_0) \propto E/T^2$ is the better fit. On both plots straight lines can be seen with a suitable figure zoom. This means that it is yet too early to conclude with a final non-Ohmic

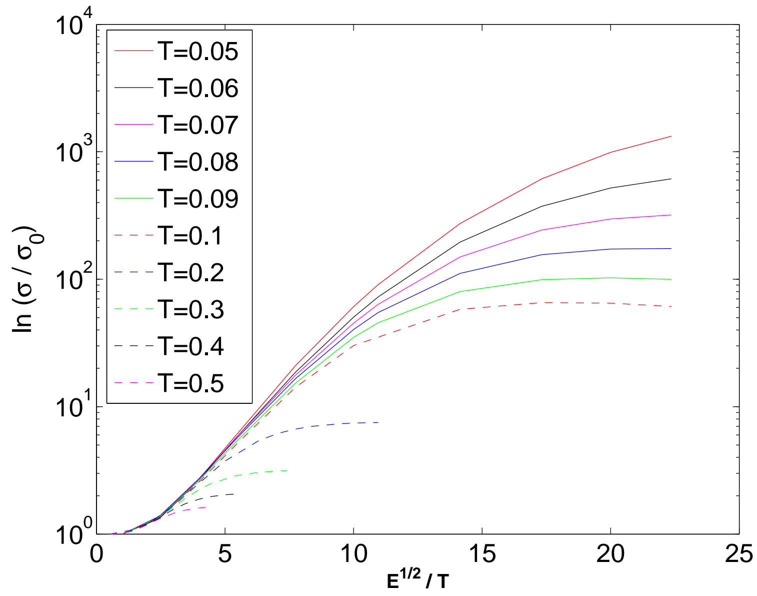

Figure 5.7: Simulation data: the logarithm of the conductivity σ as a function of $E^{1/2}/T$ at temperatures $T \in [0.05, \ \ 0.5]$ and $P_m = 50$. σ_0 is the Ohmic conductance.

$\sigma(E, T)$ dependency.

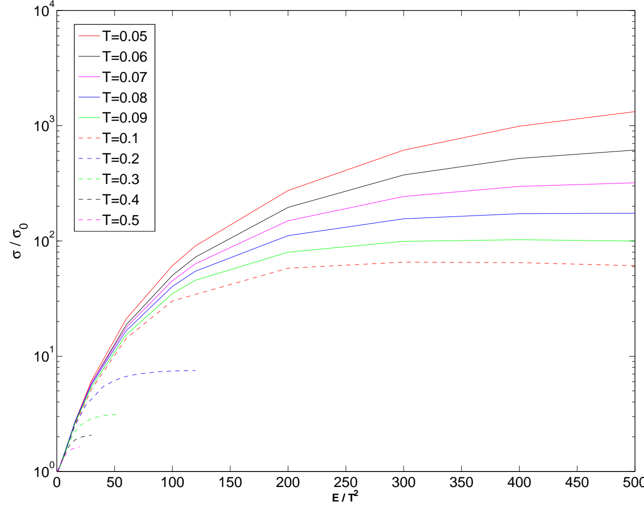

Figure 5.8: Simulation data: the logarithm of the conductivity σ as a function of E/T^2 at temperatures $T \in [0.05, \quad 0.5]$ and $P_m = 50$. σ_0 is the Ohmic conductance.

5.1 Effective Temperature in the Non-Ohmic Regime

The idea that a glass can be described by more than one temperature is not new [19]. The theoretical, numerical and to some extent experimental results suggest that glasses can possess several temperatures. The concept of the effective temperature in Coulomb glasses was introduced to us by M. Ortuño et.al [13]. In their two dimensional Coulomb glass system with impurity positional disorder they clearly see that when the system is brought out of the equilibrium by a non-Ohmic electric field, the site occupancy probability distribution follows a Fermi Dirac distribution. The Fermi Dirac distribution is characterised by an effective temperature T_{eff} which is considerably higher than the phonon bath temperature T.

Our model resembles the model of M. Ortuño et.al in several ways. We therefore choose to investigate if our system shows an effective temperature in the non-Ohmic regime. We further wish to come closer to finding a relation between the effective temperature and the electctric field. This we try to do by investigating the system's heat dissipation.

5.1.1 Estimation of the Effective Temperature T_{eff}.

To obtain the estimates of the effective temperatures we look at the impurities' occupation numbers n_i and single particle energies ε_i. From the data we obtain the probability f of a site with a certain energy being occupied. The function f follows a Fermi-Dirac distribution, from which the effective temperature T_{eff} is extracted. The details of the approach are given below:

The calculations of T_{eff} are done with 8 disorder energy samples for the temperatures

$$T \in [0.05, 0.09]$$

with field strengths in the interval

$$E \in T^2 \cdot [0.25,\ 500] \quad .$$

For temperatures

$$T \in [0.1,\ 0.5]$$

the calculations are done with 4 samples and field strengths of

$$E = T^2 \cdot [1, 6, 16, 30, 60, 100, 120, 200, 300, 400, 500]$$

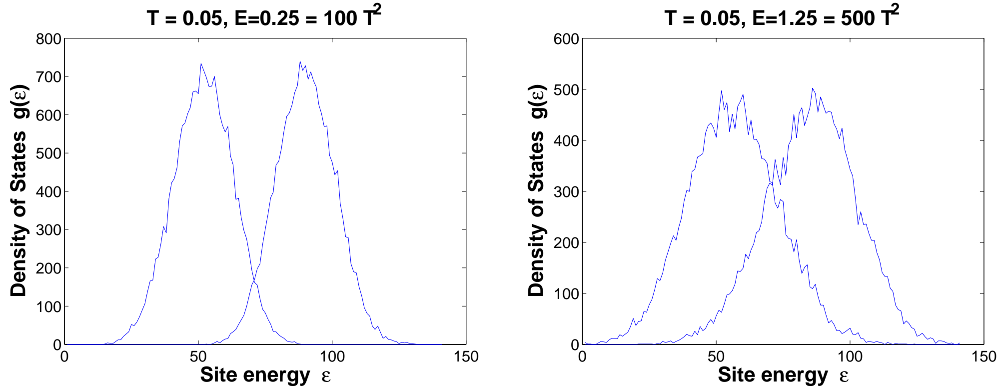

Figure 5.9: The density of states in strong, non-Ohmic fields: E=100T^2 and E=500T^2 at T=0.05.

We separate the single particle energies of occupied and empty sites into two arrays: $m(i)_{full}$ and $m(i)_{empty}$. i is the array entry number and $m(i)_{full}$ are

the array entries, which contain the number of occupied single particle energy states within a small energy interval. Correspondingly $m(i)_{empty}$ are the array entries with the number of vacant single particle states within a small energy interval. The histogram of these arrays is shown in figure 5.9. This is the system's density of states. In both graphs of figure 5.9 the leftmost "hill" represents the occupied states, whereas the rightmost "hill" represents the empty states. At their overlap the Coulomb gap is visible. The smearing of the gap is observed as the field strength increases. This indicates an increased electron temperature. The probability distribution of a site being occupied is then obtained from the creation of a new array where the entries are given by

$$f(i) = \frac{m(i)_{full}}{m(i)_{full} + m(i)_{empty}} \quad . \tag{5.3}$$

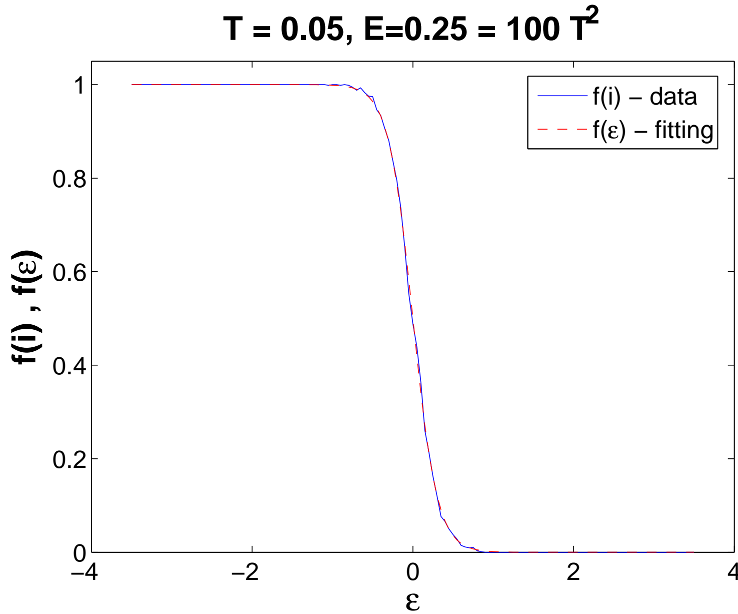

Figure 5.10: Simulation and fitting of the site occupation probability distribution. The shape resembles well the Fermi-Dirac distribution.

The plot of the data $f(i)$ and the fit $f(\varepsilon)$ is shown for T=0.05 and 2 field strengths in figures 5.10 and 5.11. The dashed line is the Fermi distribution with the effective temperature T_{eff} extracted from the data in $f(i)$. How well the site occupancy $f(i)$ fits the Fermi distribution depends on

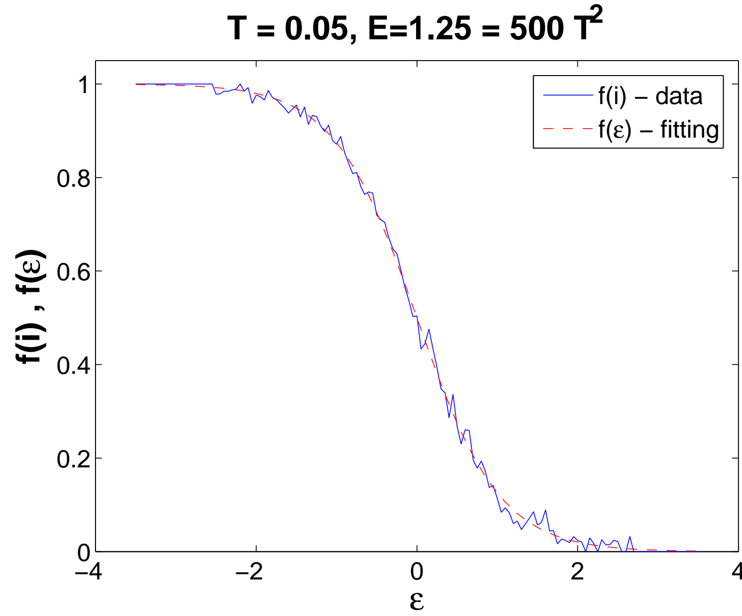

Figure 5.11: Simulation and fitting of the site occupation probability distribution for an extremely high field strength. For the low temperature of $T = 0.05$ *the shape still resembles the Fermi-Dirac distribution well and the noise is still negligible.*

the field strength and temperature. At high temperatures and strong fields ($T \geq 0.1, \quad E \sim 2$) the site occupancy probability $f(i)$ still resembles the shape of the Fermi-Dirac distribution, but has a lot of noise. This makes it difficult to determine the T_{eff} for the highest temperatures at the strongest fields.

Extraction of the T_{eff}.

It is possible to find T_{eff} by integrating the Fermi distribution as done in the equation (5.4). The Boltzmann constant is set to $k_B = 1$.

$$I = \int_0^\infty \frac{1}{e^{\varepsilon/T_{eff}} + 1} d\varepsilon \tag{5.4}$$

The evaluation is done by substituting $u = e^{\varepsilon/T_{eff}} + 1$. From this we get the following expression:

$$I = T_{eff} \int_2^\infty \frac{1}{u} \cdot \frac{1}{u-1} du = T_{eff} \int_2^\infty \frac{1}{u-1} - \frac{1}{u} du = T_{eff} \cdot ln2 \tag{5.5}$$

$$\rightarrow T_{eff} = \frac{I}{ln2} \tag{5.6}$$

In practise we perform numerical summation of the data in $f(i)$. The integral I is evaluated from the data in $f(i)$ and from the fact that

$$I_a = \int_{-\infty}^0 (1 - f(\varepsilon))\ d\varepsilon \ = \ I_b = \int_0^\infty f(\varepsilon)\ d\varepsilon \quad . \tag{5.7}$$

Assume the array $f(i)$ has N entries, then our numerical integrals $I_a \approx I_1$, $I_b \approx I_2$ are

$$I_1 = \delta\varepsilon \sum_{i=1}^{i=N/2} (1 - f(i)) \quad I_2 = \delta\varepsilon \sum_{i=N/2}^{i=N} f(i) \tag{5.8}$$

Where $\delta\varepsilon$ is the width of the numerical integration step. The estimated effective temperature T_{eff}^{est} by this method is the given by:

$$\rightarrow T_{eff}^{est} = \frac{1}{2} \cdot \frac{I_1 + I_2}{ln2} = \frac{I_1 + I_2}{ln4} \tag{5.9}$$

The error in estimation of T_{eff}.

The value of f of an unsifted Fermi-function at origo is $f(\varepsilon = 0) = 0.5$. The Fermi functions from the simulation data can be shifted by $\Delta\varepsilon$ to the left or right with respect to origo. In a finite system the single particle energies and the electron configurations will fluctuate from sample to sample.

This causes the shift in $f(i)$ and an error in the estimate of T_{eff}. The shift causes an uncertainty in all the first half entries in the $f(i)$ array having values bigger than or equal to 0.5.

$$i \in \Big[0, \frac{N}{2}\Big], \quad f(i) \geq 0.5$$

It is also not certain that all the entries in the latter half of the array are smaller than or equal to 0.5:

$$i \in \Big[\frac{N}{2}, N\Big], \quad f(i) \leq 0.5$$

Below an estimate of the error in T_{eff} due to the shift of the Fermi function with respect to origo is given.

Error in T_{eff} due to the shift $\Delta\varepsilon$ of the Fermi Function.

We evaluate the integrals in equation (5.7) taking the shift $\Delta\varepsilon$ into account and insert the results into equation (5.9). We choose a situation where the Fermi curve is shifted to the left of origo. We start with evaluating I_b:

$$I_b = \int_{-\Delta\varepsilon}^{\infty} \frac{1}{e^{\varepsilon/T_{eff}} + 1} d\varepsilon \tag{5.10}$$

The above integral is evaluated by substitution:
$u = e^{\varepsilon/T_{eff}} + 1$ and $d\varepsilon = \frac{T_{eff}}{u-1} du$.

$$I_b = \int_{e^{-\Delta\varepsilon/T_{eff}}+1}^{\infty} \frac{1}{u} \cdot \frac{T_{eff}}{u-1}\, du = -T_{eff} \int_{e^{-\Delta\varepsilon/T_{eff}}+1}^{\infty} \frac{1}{u} - \frac{1}{u-1}\, du$$

$$I_b = -T_{eff} \Big[\, ln\Big(\frac{u}{u-1}\Big)\, \Big]_{e^{-\Delta\varepsilon/T_{eff}}+1}^{\infty} = T_{eff}\; ln\; \Big(\frac{e^{-\Delta\varepsilon/T_{eff}}+1}{e^{-\Delta\varepsilon/T_{eff}}} \Big)$$

$$I_b = T_{eff} ln\Big(1 + e^{\Delta\varepsilon/T_{eff}}\Big) \tag{5.11}$$

We evaluate the integral I_a:

$$I_a = \int_{-\infty}^{-\Delta\varepsilon} 1 - \frac{1}{e^{\varepsilon/T_{eff}} + 1} d\varepsilon = \int_{-\infty}^{-\Delta\varepsilon} \frac{e^{\varepsilon/T_{eff}}}{e^{\varepsilon/T_{eff}} + 1} d\varepsilon \tag{5.12}$$

The first substitution $\Delta\varepsilon = -\Delta\varepsilon$ and $d\varepsilon = -d\varepsilon$ gives the following expression for I_a:

$$I_a = \int_{\Delta\varepsilon}^{\infty} \frac{1}{e^{\varepsilon/T_{eff}} + 1} d\varepsilon \tag{5.13}$$

The second substitution with $u = e^{\varepsilon/T_{eff}} + 1$, $d\varepsilon = T_{eff}\frac{du}{u-1}$ results in an integral which is equal with I_b except the limits. The further method of evaluation of I_a is therefore the same as for I_b.

$$I_a = -T_{eff} \int_{e^{\Delta\varepsilon/T_{eff}}+1}^{\infty} \frac{1}{u} - \frac{1}{u-1}\, du = -T_{eff}\left[ln\left(\frac{u}{u-1}\right) \right]_{e^{\Delta\varepsilon/T_{eff}}+1}^{\infty}$$

$$I_a = -T_{eff}\left[0 - ln\left(\frac{e^{\Delta\varepsilon/T_{eff}} + 1}{e^{\Delta\varepsilon/T_{eff}}}\right)\right] = T_{eff}\; ln\left(1 + e^{-\Delta\varepsilon/T_{eff}}\right)$$

$$I_a = T_{eff} ln\left(1 + e^{-\Delta\varepsilon/T_{eff}}\right) \tag{5.14}$$

We insert equations (5.11) and (5.14) into (5.9). T_{eff} is the correct effective temperature of the system and T_{eff}^{est} is the estimated effective temperature from our approach.

$$T_{eff}^{est} = \frac{T_{eff} ln\left(1 + e^{-\Delta\varepsilon/T_{eff}}\right) + T_{eff} ln\left(1 + e^{\Delta\varepsilon/T_{eff}}\right)}{2ln2} \tag{5.15}$$

$$T_{eff}^{est} = T_{eff} \cdot \frac{ln\left(2 + 2\cosh(\frac{\Delta\varepsilon}{T_{eff}})\right)}{ln4} \tag{5.16}$$

From equation (5.16) we see that a shift of the Fermi curve in either direction gives an estimated effective temperature which is higher than the correct effective temperature. $\Delta\varepsilon \neq 0 \rightarrow T_{eff}^{est} > T_{eff}$.

How the shift is found:

If there is no shift in the data set, then the Fermi curve should cross the y-axis at 0.5: $f(\varepsilon = 0) = 0.5$. If there is a shift of $\Delta\varepsilon$, then $f(\Delta\varepsilon) = 0.5$. We therefore find the two points in the data set of the Fermi distribution closest to 0.5, do a linear interpolation of these by a simple, self-made matlab-program and estimate she shift $\Delta\varepsilon$:

If $(\varepsilon_1, f(\varepsilon_1))$ and $(\varepsilon_2, f(\varepsilon_2))$ are the points we interpolate by a straight line

$f(\varepsilon) = a\varepsilon + b$, then the slope is $a = (f(\varepsilon_2) - f(\varepsilon_1))/(\varepsilon_2 - \varepsilon_1)$ and the y-intercept is $b = f(\varepsilon_1) - a\varepsilon_1 = f(\varepsilon_2) - a\varepsilon_2$. The estimated shift $\Delta\varepsilon$ is then given by

$$\Delta\varepsilon = \frac{0.5 - b}{a} \tag{5.17}$$

From our data, for the lowest temperatures and the weakest to intermediate field strengths,$E \leq 100T^2$, we read off a shift of the order

$$\Delta\varepsilon \approx 10^{-3}$$

with

$$\Delta T_{eff}^{shift} \approx 10^{-4} \quad .$$

For the strongest fields

$$\Delta\varepsilon \approx 10^{-2}$$

with

$$\Delta T_{eff}^{shift} \approx 10^{-3} \quad .$$

An exception occurs for $T = 0.09$; for $E \geq 30T^2$ shifts of $\Delta\varepsilon \approx 10^{-1}$ with $\Delta T_{eff}^{shift} \approx 10^{-1}$ are observed. These deviations are clearly seen in figure 5.12.

For the highest temperatures and the weakest fields the shift is

$$\Delta\varepsilon \approx 10^{-3} - 10^{-2}$$

with $\Delta T_{eff}^{shift} \approx 10^{-5} - 10^{-4}$. For the strongest fields $\Delta\varepsilon \approx 10^{-2}$ with

$$\Delta T_{eff}^{shift} \approx 10^{-4} \quad .$$

For each temperature the error estimates ΔT_{eff}^{shift} are calculated from (5.16) with the lowest possible effective temperature $T_{eff} = T$.

The error in T_{eff} due to numerical integration.

The standard error of the mean value in the estimates of the effective temperature is given by

$$\sigma_{T_{eff}} = \frac{\Delta_{T_{eff}}}{\sqrt{N}} \quad .$$

Where ΔT_{eff} is the standard error in a single measurement and N is the number of measurements. When using the summation in equation (5.8) instead of evaluating the actual integration in equation (5.5), the numerical integration increases the error in the estimates of T_{eff}. This means that there also is a contribution to the standard error from the numerical integration error ΔT_{eff}^{num}:

$$\Delta T_{eff} = \sqrt{(\Delta T_{eff}^{shift})^2 + (\Delta T_{eff}^{num})^2}$$

Our estimates show that

$$\Delta T_{eff}^{num} \approx 10^{-3}$$

Which means that for field values $E < 100T^2$

$$\Delta T_{eff}^{shift} < \Delta T_{eff}^{num},$$

and most of the error originates from the numerical integration.

Comments on the averaging.

The averaging is done for different system configurations at different times; In the beginning of this chapter we mentioned running the programme with 8 disorder energy samples through 10 and 20 million jumps, depending on the temperature. The measurements are done after each million jumps in the steady state. We assume that when being in the steady state the system single particle energies and their occupation numbers differ enough after each million jumps to be considered as independent samples. However, for each temperature and field strength the number of disorder samples and millions of jumps vary due to various technical reasons throughout the project. Thus also the quality of the T_{eff} estimates varies. For $T \in [0.05, 0.09]$ and weak to intermediate field strengths we have many samples - approximately 144 to 200 values, which give a rather good averaging. For strong fields, $E \geq 100T^2$, some estimates have ≈ 80 samples, some have only 5 samples. For the last mentioned ones $\sigma_{T_{eff}} \approx 10^{-2}$.

For $T \in [0.1, 0.5]$ the situation is the same, but the number of samples is considerably smaller: For the lowest fields $E \leq 100T^2$ the number of samples

≈ 100, whereas for the highest fields the number is ≈ 32. To avoid confusion and messy graphs, the error bars are not included in the coming plots.

Analysis of the plots:

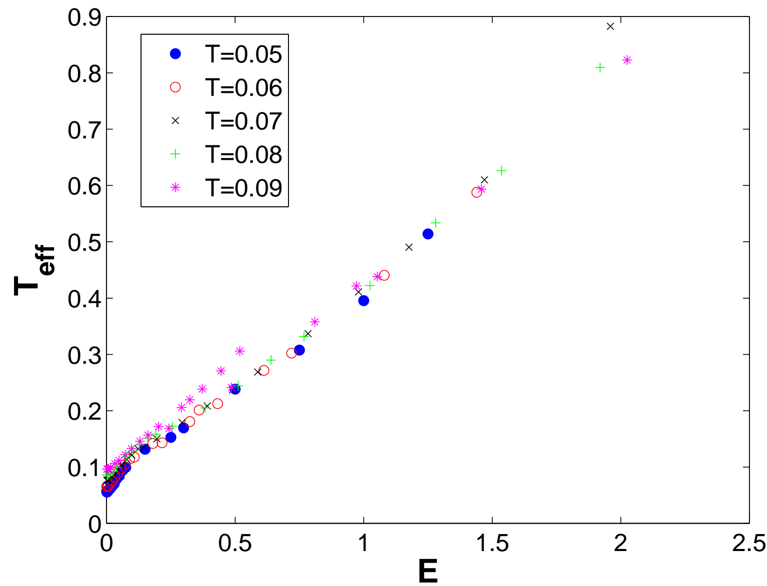

Figure 5.12: Effective temperature as a function of the non-Ohmic field strength for the lower temperatures $T \in [0.05,\ 0.09]$.

Figure 5.12 shows the effective temperatures of $T \in [0.05, 0.09]$ as the field strength is increased. Figure 5.13 is a zoom-in on the lower left corner of figure 5.12. Figure 5.14 shows the effective temperatures versus increasing field strength for the higher temperatures $T \in [0.1, 0.5]$.

In general we observe that the effective temperature increases as the field strength increases. At a certain field strength the graphs seem to be on their way of merging together. For all temperatures it looks like with high field strengths the system can be characterized by the same effective temperature and yet have different phonon bath temperatures. The estimates for

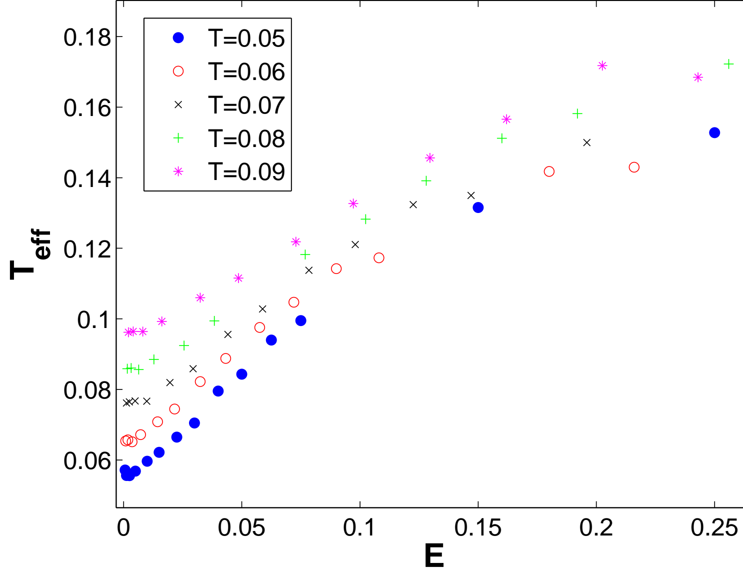

Figure 5.13: A zoom-in on figure 5.12.

$T = 0.09$ in figure 5.12 deviate from the other low temperature estimates. These are averages of 144 measurements for intermediate field strengths. The resemblance with the Fermi-Dirac distribution and the averaging has been checked. The deviation is probably due to the considerable shift $\Delta\varepsilon \approx 10^{-1}$ of the Fermi curve.

Another interesting point is shown in figure 5.15. The graphs display the corresponding conductivity and effective temperature values at intermediate non-Ohmic field strengths. These are plotted together with the Ohmic values from figure 4.7 where $T_{eff} \approx T$, as discussed in section 4.4. As the field and hence the effective temperature increase, the system's conductivity seems to behave as though the system's temperature were higher than the phonon bath temperature. For strong fields or high real temperatures the $\sigma(T_{eff})$ dependency resembles the Ohmic one.

The figures discussed above open up for questions like:
"What is the relation between T, E and T_{eff}?" and "How does the field strength affect the non-Ohmic conductivity expressed by the effective temperature?" I.e "What is the relation between σ and T_{eff}?" To be able to

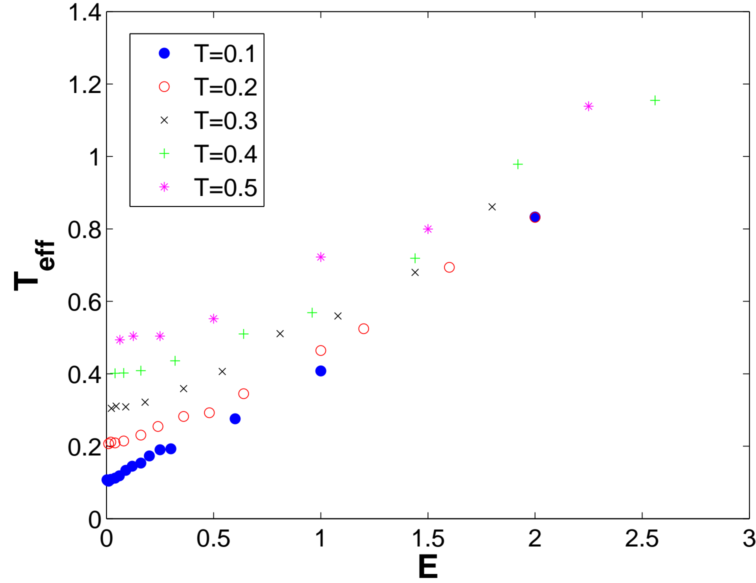

Figure 5.14: Effective temperature as a function of the non-Ohmic field strength for the higher temperatures $T \in [0.1,\ 0.5]$.

make theoretical predictions, a further thorough research of the system is needed. In next section we take a look at the heat dissipation of the system, which we believe can bring us closer to answering the above questions.

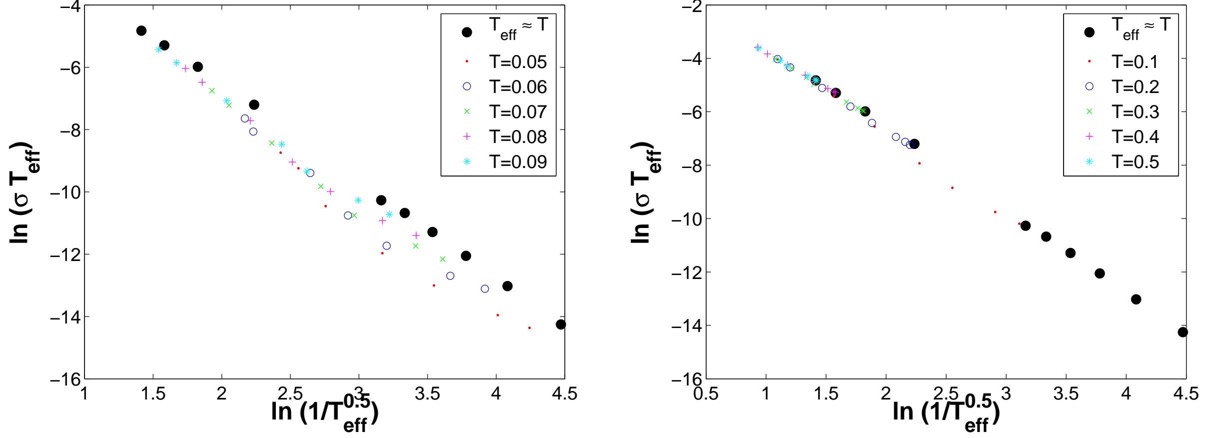

Figure 5.15: The Efros-Shklovskii Law for the effective temperature. The leftmost graph - the conductivity as function of $Teff$ for low temperatures. $E = T^2[1, 6, 16, 30, 60, 100, 120]$. The rightmost graph - the conductivity as function of T_{eff} for high temperatures $E \in T^2[0.25, 120]$.

5.2 The System Heat Dissipation.

We would like to find the relation between the effective temperature T_{eff} and the electric field E, which later can be connected to $\sigma(T_{eff})$. This may be possible by investigating the heat dissipation of the system. Below, the very beginning of this research will be introduced. Figure 5.16 shows the system energy transfer where $P_{ph\to e}$ is the power the lattice electrons absorb from the phonon bath, P_{field} is the power the electrons absorb from the electric field and $P_{e\to ph}$ is the power the electrons emit into the phonon bath. In a situation with no field present the energy exchange between the electrons and the phonon bath should be equal. When the electric field is present it transfers energy into the lattice. The energy the electrons emit into the phonon bath should be equal to the energy they absorb from the electric field and the phonon bath. This means that there is an energy relation:

$$P(T, T_{eff})_{ph\to e} + P(E, T_{eff})_{field} = P(T, T_{eff})_{e\to ph} \tag{5.18}$$

Both situations are confirmed by an analysis of our data:
Figure 5.17 shows emitted and absorbed power versus real temperature in the absence of the electric field. The plots overlap and are difficult to distinguish. Hence $P_{ph\to e} \approx P_{e\to ph}$. The relative difference between the absorbed

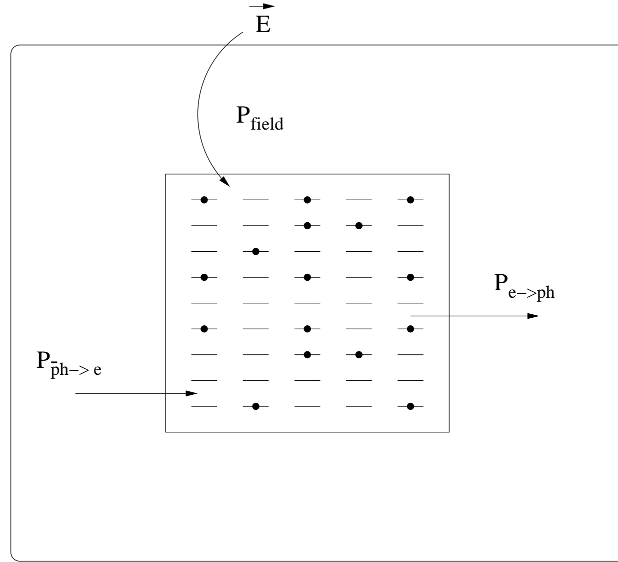

Figure 5.16: The energy transfer in the system. The lattice absorbs energy (power) from the phonon bath $P_{ph\rightarrow e}$ and the electric field P_{field}, and emits energy back into the phonon bath $P_{e\rightarrow ph}$.

and emitted power $\dfrac{(P_{ph\rightarrow e} - P_{e\rightarrow ph})}{P_{e\rightarrow ph}}$ is shown in the leftmost graph in figure 5.18. It confirms the equation (5.18) in cases with no electric field.

The rightmost graph in figure 5.18 shows a linear fit to the logarithmic plot of the points in figure 5.17. It is possible to assume that in equilibrium the $P_{e\rightarrow ph}$ and $P_{ph\rightarrow e}$ obey some law like

$$P_{e\rightarrow ph} \sim P_{ph\rightarrow e} \sim T^{\alpha} \tag{5.19}$$

with the slope of $\alpha \approx 3.7$. The situation gets more complicated as soon as the energy contribution from the electric field is included.

The leftmost graph in figure 5.19 shows that in the presence og the electric field the power emitted by the system $P_{e\rightarrow ph}$ increases as the field strength increases due to the field energy supply. The power absorbed by the electrons from phonons is the same as in the case with no field. The rightmost

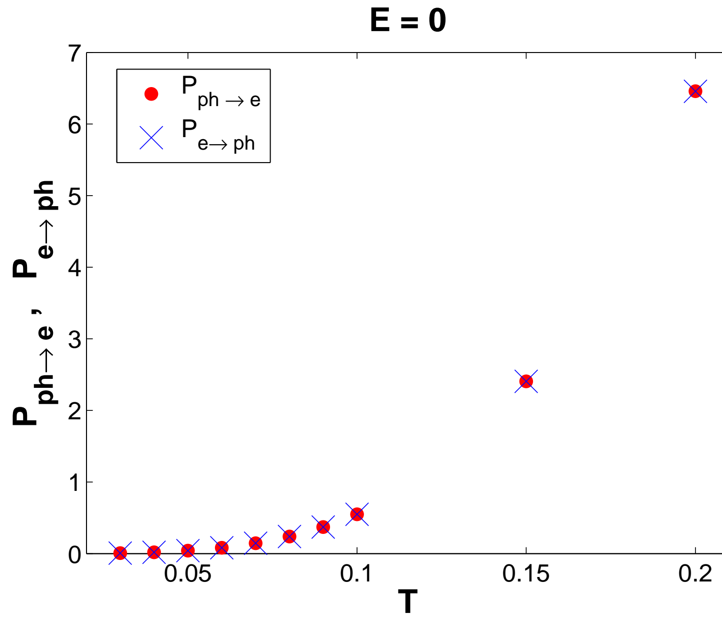

Figure 5.17: $P_{ph\to e}$ *- dots,* $P_{e\to ph}$ *- crosses.*
$P_{ph\to e} \approx P_{e\to ph}$ *when there is no electric field.*

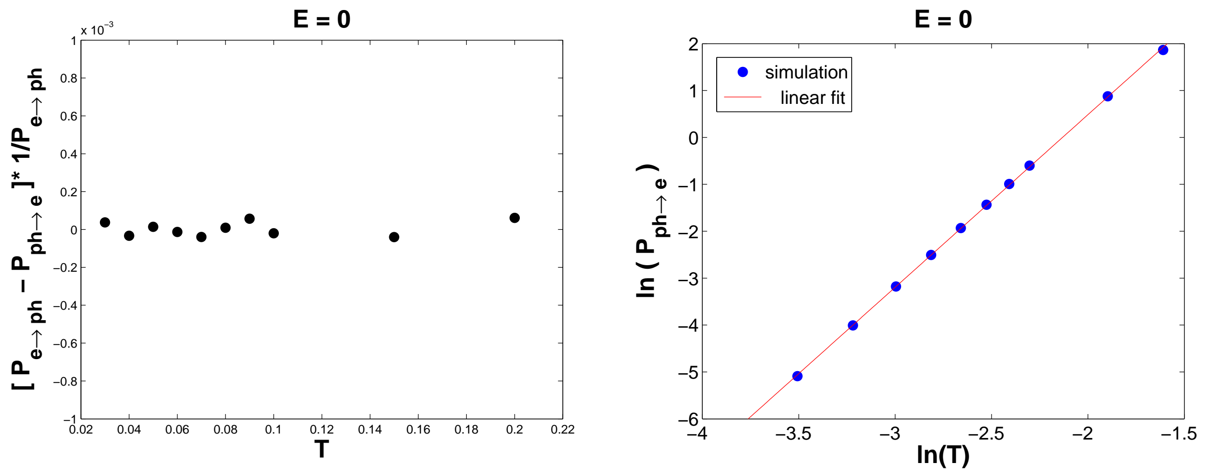

Figure 5.18: Left: The relative difference between the absorbed and emitted power.
Right: Linear fit to the logarithm of the data in figure 5.17.

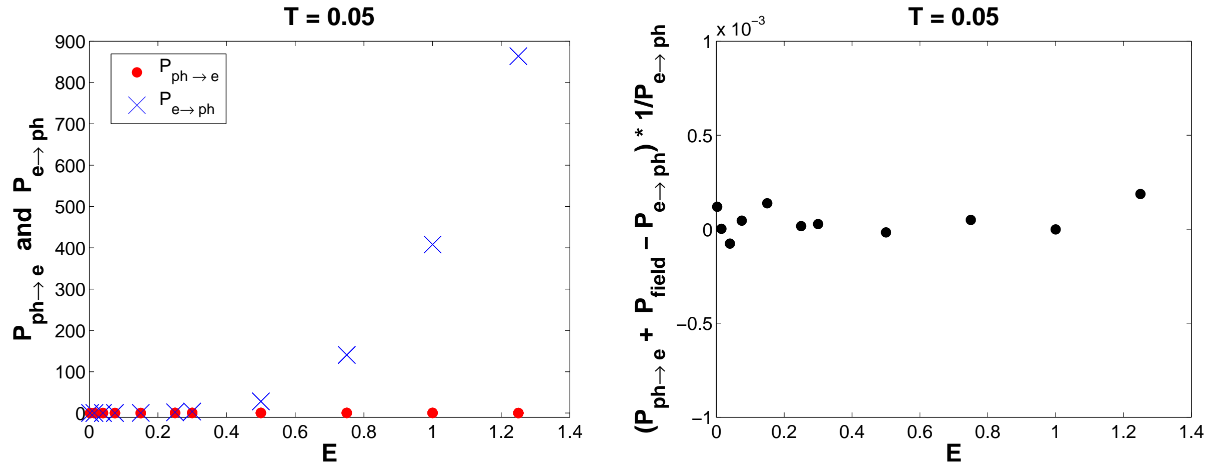

Figure 5.19: Left: Absorbed energy from the phonon bath - dots. Emitted energy - crosses. The emitted energy is much bigger than the one absorbed from the phonons due to the field energy supply.
Right: The relative difference between the total absorbed and emitted power in the system with the electric field present.

graph in figure 5.19 shows the relative difference between the points in figure 5.19 and confirms the equation (5.18). Equal results are obtained for all the temperatures: $T \in [0.05,\ 0.5]$.

5.2.1 Heat emission map

We also investigated the heat emission of the system, shown in figure 5.20. The map shows how much net energy is emitted at each lattice point during the last million in a 20-million jump session.

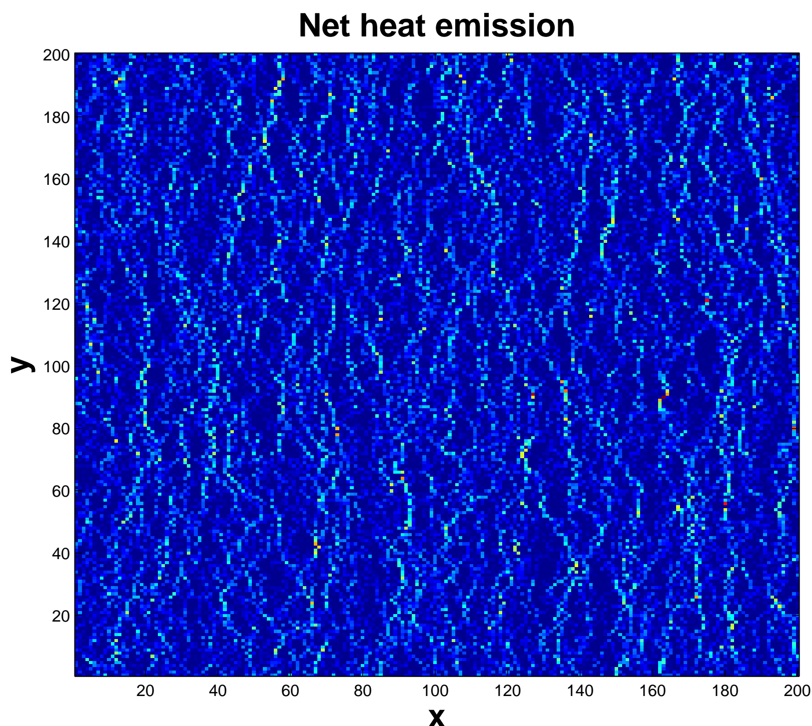

Figure 5.20: Heat emission map for a 200×200 *system with* $T = 0.05$ *and* $E_x = 0.25 = 100T^2$.

By making heat emission map it is possible to see whether the energy is emitted homogeneously or there are "hot spots" in the system. This kind of information is important for the establishment of analytical models. Often, but not necessarily, the presence or absence of hot spots and their aspect ratio are related with the current voltage curves of the system. Surprisingly we observe stripes directed perpendicularly to the field direction. We ran a similar calculation with the field directed in the y-direction in order to check whether the stripes were a programme artefact. We observe similar stripes,

but in x-direction, again perpendicularly to the field. These results are beyond our current comprehension. The heat emission pattern also remains as an open question.

Chapter 6

Discussion

Throughout this project we investigated the low temperature transport properties of a 2 dimensional semiconductor system. The system had Anderson localization, long range Coulomb interactions, and was influenced by an electric field. We performed research on both the weak field, Ohmic region, and the strong field, non-Ohmic region.

In the Ohmic region we established the values of several important parameters like the suitable temperature interval of $T \in [0.05,\ 0.5]$, the approximate Ohmic regime of $E \leq \frac{T}{10}$ and the system size of $L = 100$ for the highest temperatures in the interval and $L = 200$ for the lowest temperatures. By calculating the temperature dependent conductivity with the chosen parameters we observed the Coulomb gap in the density of states as predicted by the Efros-Shklovskii law of $\sigma(T) = \sigma_0(T)\exp[-(T_0/T)^{1/2}]$ for variable range hopping. We also observed that our data fit best with the prefactor being temperature dependent $\sigma_0 \sim \frac{1}{T}$.

In the non-Ohmic regime we observed a peculiar decrease in the conductivity after a certain field limit. We understood that this was due to the activation rate cut-off parameter P_m and have now a clearer picture of how this parameter is related to the DeBye frequency and how it affects the conductivity behaviour. By being aware of the choice of P_m we compared our strong field results with the well known experiments done by Aronzon et al. From these we see that $\ln\sigma(E,T) \sim \frac{E^{1/2}}{T}$ or $\ln\sigma(E,T) \sim \frac{E}{T^2}$ rather than $\ln\sigma(E,T) \sim \frac{E}{T}$.

We also observed a heating of the electrons by the field and that the system can be described by two temperatures - a real phonon bath temperature T and an effective electron temperature T_{eff}. This can be seen from

the system's site occupation probability distribution function following a Fermi-Dirac distribution from which a higher effective temperature can be extracted. We saw interesting results in the relation between E, T_{eff} and σ which we tried to understand by investigating the energy transfer and the heat emission of the system. We have confirmed the system absorbing energy from the electric field and the phonon bath and emitting an equal amount of energy back into the phonon bath. We further made a heat emission map of the lattice. We expected to find either homogeneous emission or hot spots. Instead we observed peculiar "heat stripes" directed perpendicularly to the field direction.

Future work

The research of the relation between E, T, σ and the heat emission in the non-Ohmic fields is in the early stage and needs further development. In addition to the work described in the thesis we investigated several other interesting aspects, which unfortunately the time didn't allow us to finish. Some of these are mentioned below. We did research on the calculation of the temperature dependent conductivity in the Ohmic regime by using the Fluctuation Dissipation Theorem. This theorem states that the conductivity can be found from the fluctuations of a system in equilibrium. We have tried to do so by analyzing the current correlation functions, but haven't obtained any reasonable results. We also began expanding our programme to 3 dimensions. The idea was to perform the analysis of chapter 4 on a 3 dimensional system. A third aspect we didn't yet succeed in showing is Mott's prediction of the increasing average electron jumping length with decreasing temperature. By ordinary averaging we observed a contrary behaviour; the average jump length decreased with decreasing temperature. We realised that ordinary averaging of the jump lengths is not a satisfactory procedure because of the presence of close pairs of sites with close single particle energies, between which transitions are highly probable. As the temperature decreases these pairs dominate the jumps with one electron jumping back and forth between such sites with no net current contribution. By omitting these kind of pairs in the calculation of the average jumping length and weighting the average length by the current passing through the link, we still don't see the desired increase. However the the average jumping length became essentially temperature independent.

Appendix A

Miller-Abrahams Hopping Rate

A derivation of the hopping rate will be given below. The original derivation demands many calculations [5]. Here a summary is provided.

Consider 2 donors i and j with spatial coordinates $\vec{r_i}$ and $\vec{r_j}$. The donors are surrounded by many other charged impurities which set up local, fluctuating potentials. $W(\vec{r_i})$ represents the strong interactions between a donor and its fluctuating surroundings. The distance between the donors is much bigger than the localization radius $r_{ij} >> a$. The impurity wave functions $\Psi_i(\vec{r})$, $\Psi_j(\vec{r})$ are assumed to be hydrogen-like, as given in equation A.1, and have a small overlap I_{ij}.

$$\Psi(\vec{r}) \sim F(\vec{r}) = \frac{1}{\sqrt{\pi a^3}}\ e^{-\vec{r}/a} \quad ground \ \ state \tag{A.1}$$

The interactions between the electrons and the surrounding impurities splits the degenerate donor states and alters the potential wells. The overlap for hydrogen-like functions which are obtained by the LCAO-method, can be evaluated and is given by

$$I_{ij} = \int \Psi_i^* \Psi_j \frac{e^2}{\kappa|\vec{r} - \vec{r_i}|} d\vec{r} - \int \Psi_i^* \Psi_j d\vec{r'} \int \frac{e^2 |\Psi_i|^2}{\kappa|\vec{r} - \vec{r_i}|} d\vec{r} \tag{A.2}$$

$$I_{ij} = \frac{2}{3} \frac{e^2}{\kappa a^2} r_{ij} e^{-r_{ij}/a} \tag{A.3}$$

It is then possible to use the system Hamiltonian (A.4)

$$\mathcal{H} = \mathcal{H}_0 - \frac{e^2}{\kappa|\vec{r} - \vec{r_i}|} - \frac{e^2}{\kappa|\vec{r} - \vec{r_j}|} + W(\vec{r_i}) + W(\vec{r_j}) \tag{A.4}$$

to calculate the impurity wave functions by taking the overlap and the interaction with the surroundings into account. The first term is the periodic lattice Hamiltonian (1.1), the next two terms are the impurity potentials and the last two terms are contributions from the surroundings on each of the two impurities.

When the dopant concentration is low and the interaction with the local surroundings $\Delta_{ij} = W(\vec{r_j}) - W(\vec{r_i})$ is bigger than the overlap $\Delta_{ij} >> I_{ij}$, the wave functions differ little from the isolated donor wave functions:

$$\Psi_i^{'} = \Psi_i + \frac{I_{ij}}{\Delta_{ij}}\Psi_j \tag{A.5}$$
$$\Psi_j^{'} = \Psi_j - \frac{I_{ij}}{\Delta_{ij}}\Psi_i$$

It is further possible to show that the energy difference between the states with wave functions $\Psi_i^{'}$ and $\Psi_j^{'}$ is $\approx \Delta_{ij}$, which means that in the transition between the states a phonon of energy Δ_{ij} must either be emitted or absorbed. The phonon energy is usually a few meV. Miller & Abrahams assume that the electrons only interact with one acoustic phonon branch with an isotropic energy spectrum and a linear dispersion relation

$$\omega = s \cdot q \tag{A.6}$$

where s is the speed of sound in the medium and q is the phonon wave vector. To obtain the transition probability the matrix element of the electron-phonon interaction $\langle H^{'}\rangle$ is calculated by the deformation theorem. This theorem applies the effective mass method which is extended to gradual shifts in energy bands. The shifts result from deformation of the crystal lattice during the lattice-phonon interactions [20].

$$\langle H^{'}\rangle = \langle\Psi_j^{'}|H^{'}|\Psi_i^{'}\rangle = iE_1\Big(\frac{\hbar q N}{2\rho_0 V s}\Big)^{1/2}\int \Psi_j^{'} e^{i\vec{q}\cdot\vec{r}}\Psi_i^{'}\ d\vec{r} \tag{A.7}$$

where E_1 is a constant describing the deformation potential, $\eta = i(\frac{\hbar}{2\rho_0 V s})^{1/2}$ is the dilation, N is the Planck distributions and $\rho_0,\ V,\ s$ are the lattice density, volume and the longitudinal sound velocity. After several calculation steps and eliminating small terms the matrix element is given by

$$\langle H^{'}\rangle = iE_1\Big(\frac{\hbar q N}{2\rho_0 V s}\Big)^{1/2}\frac{I_{ij}}{\Delta_{ij}}\Big[\int F_j^2 e^{i\vec{q}\cdot\vec{r}}\ d\vec{r} - \int F_j^2 e^{i\vec{q}\cdot\vec{r}} d\vec{r}\Big] \tag{A.8}$$

The hydrogen-like wave functions F_i and F_j being identical permits to write $F_j(\vec{r}-\vec{r}_{ij}) = F_i(\vec{r})$. (A.8) is then

$$\langle H' \rangle = iE_1\Big(\frac{\hbar q N}{2\rho_0 V s}\Big)^{1/2}\frac{I_{ij}}{\Delta_{ij}}(e^{i\vec{q}\cdot\vec{r_{ij}}}-1)\int F_i^2 \quad e^{i\vec{q}\cdot\vec{r}}d\vec{r} \tag{A.9}$$

Calculation of $\int F_i^2 \quad e^{i\mathbf{q}\cdot\mathbf{r}}d\mathbf{r}$

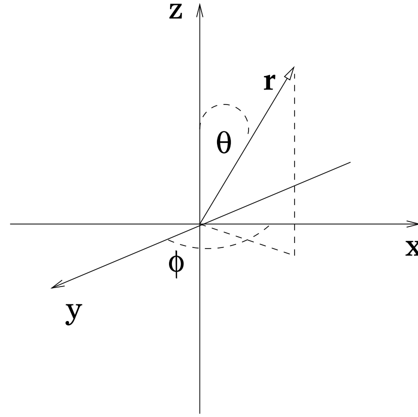

Figure A.1: Spherical coordinates chosen for the integration

We calculate the integral by using spherical coordinates and the ground state hydrogen-like wave function from equation (A.1).

$$\begin{aligned}\int F_i^2 \quad e^{i\vec{q}\cdot\vec{r}}d\vec{r} &= \frac{1}{\pi a^3}\int_{\varphi=0}^{2\pi}\int_{\theta=0}^{\pi}\int_{r=0}^{\infty} e^{-2r/a}\cdot e^{iqr\cos\theta}\ r^2\sin\theta\ dr\ d\theta\ d\varphi \\ &= \frac{2}{a^3}\int_{r=0}^{\infty} e^{-2r/a}\ r^2\ dr\int_{\theta=0}^{\pi} e^{iqr\cos\theta}\sin\theta\ d\theta \end{aligned}\tag{A.10}$$

The inner integral is solved by substituting $u = \cos\theta$

$$\int_{-1}^{1} e^{iqru}du = \frac{1}{iqr}\Big(e^{iqr}-e^{-iqr}\Big) \tag{A.11}$$

Inserting (A.11) into (A.10) and rearranging we get:

$$\int F_i^2 \quad e^{i\vec{q}\cdot\vec{r}} d\vec{r} = \frac{2}{iqa^3}\left[\int_0^\infty r\ e^{-r\left(2/a-iq\right)}\ dr - \int_0^\infty r\ e^{-r\left(2/a+iq\right)}\ dr\right] \tag{A.12}$$

The integrals in (A.12) are solved by the known result of

$$\int_0^\infty x^n e^{-x/b}\ dx = n!\ b^{n+1} \tag{A.13}$$

$$\begin{aligned}\int F_i^2 \quad e^{i\vec{q}\cdot\vec{r}} d\vec{r} &= \frac{2}{iqa^3}\left(\frac{a}{2}\right)^2\left[\frac{1}{\left(1-\frac{iqa}{2}\right)^2} - \frac{1}{\left(1+\frac{iqa}{2}\right)^2}\right] \\ &= \frac{2}{iqa^3}\left(\frac{a}{2}\right)^2\left[\frac{2iqa}{\left(1-\frac{iqa}{2}\right)^2\left(1+\frac{iqa}{2}\right)^2}\right] \\ &= \frac{1}{\left[1+(\frac{qa}{2})^2\right]^2}\end{aligned} \tag{A.14}$$

Inserting (A.14) into (A.9) and complex conjugating one obtains

$$|\langle H^{'}\rangle|^2 = \frac{\hbar q E_1^2}{\rho_0 V s}\frac{I_{ij}}{\Delta_{ij}} N(1 - cos(\vec{q}\cdot\vec{r}_{ij}))\left[1+(\frac{qa}{2})^2\right]^{-4} \tag{A.15}$$

The $\cos(\vec{q}\cdot\vec{r}_{ij}) \approx 0$ due to big values of qr_{ij}. The jumping probability γ_{ij} is given by

$$\gamma_{ij} = \frac{2\pi}{\hbar}\frac{V}{(2\pi)^3}\int |\langle H^{'}\rangle|^2 \delta(\hbar sq - \Delta_{ij}) d\vec{q} \tag{A.16}$$

In 3 dimensions the spherical coordinates give the following expression:

$$\begin{aligned}\gamma_{ij} &= \frac{2\pi}{\hbar}\frac{V}{(2\pi)^3} 4\pi \int |\langle H^{'}\rangle|^2 \delta(\hbar sq - \Delta_{ij}) q^2 dq \\ &= 4\pi\frac{2\pi}{\hbar}\frac{V}{(2\pi)^3}\frac{\hbar E_1^2}{\rho_0 V s}(\frac{I_{ij}}{\Delta_i j})^2 N \int q^3\left[1+(\frac{qa}{2})^2\right]^{-4}\delta(\hbar sq - \Delta_{ij}) dq \\ &= \frac{E_1^2 I_{ij}^2 N \Delta_{ij}}{\pi\rho_0\hbar^4 s^5}\left[1+(\frac{\Delta_{ij} a}{2\hbar s})^2\right]^{-4}\end{aligned} \tag{A.17}$$

Inserting the expression (A.3) for I_{ij} we get the final result:

$$\gamma_{ij} = \frac{E_1^2 \Delta_{ij}}{\pi \rho_0 \hbar^4 s^5} \Big(\frac{2e^2}{3\kappa a} \Big) \Big(\frac{r_{ij}}{a} \Big) \Big[1 + (\frac{\Delta_{ij} a}{2\hbar s})^2 \Big]^{-4} \ e^{-2r_{ij}/a} \ N(\Delta_{ij})$$

$$\gamma_{ij} = \gamma_{ij}^0 (\Delta_{ij}) \ e^{-2r_{ij}/a} \ N(\Delta_{ij}) \tag{A.18}$$

Bibliography

[1] N.D. Mermin N.W. Ashcroft. *Solid State Physics*. Thomson Learning, 1976.

[2] A.L. Efros B.I. Sklovskii. *Electronic Properties of Doped Semiconductors*. Springer-Verlag Berlin Heidelberg New York Tokyo, 1984.

[3] N.F. Mott. Conduction in non-crystalline materials, localized states in a pseudogap and near extremities of conduction and valence bandson-crystalline materials,localized states. *Philosophical Magazine*, 19:835–852, 1969.

[4] H. L. Frisch, J. M. Hammersley, and D. J. A. Welsh. Monte carlo estimates of percolation probabilities for various lattices. *Phys. Rev.*, 126(3):949–951, May 1962.

[5] E. Abrahams A. Miller. Impurity conduction at low concentrations. *Physical Review*, 120, 1960.

[6] N.F. Mott and E.A. Davis. *Electronic Processes in Non-Crystalline Materials, Second Edition*. Oxford Clarendon Press, 1979.

[7] A.V. Nenashev et. al. Hopping conduction in strong electric fields: Negative differential conductivity. *Physical Review B*, 78, 2008.

[8] V.V. Ryl'kov. B.A. Aronzon, D.Yu. Kovalev. Nonohmic quasi 2d hopping conductance and the kinetics of its relaxation. In *Semiconductors, No 7*, volume 39, pages 811–819. Pleiades Publishing, Inc, 2005.

[9] George D. Rose et. al. A backbone-based theory of protein folding. *PNAS*, 103, 2006.

[10] M.Ortuño et. al. Coulomb interactions in anderson insulators. *Philosophical Magazine*, 81(9):1049–1064, 2001.

[11] D. N. Tsigankov, E. Pazy, B. D. Laikhtman, and A. L. Efros. Long-time relaxation of interacting electrons in the regime of hopping conduction. *Phys. Rev. B*, 68(18):184205, Nov 2003.

[12] D. N. Tsigankov and A. L. Efros. Variable range hopping in two-dimensional systems of interacting electrons. *Phys. Rev. Lett.*, 88(17):176602, Apr 2002.

[13] A. M. Somoza, M. Ortu no, M. Caravaca, and M. Pollak. Effective temperature in relaxation of coulomb glasses. *Physical Review Letters*, 101(5):056601, 2008.

[14] Martin Kirkengen. *Collective Electron Properties of Hopping Insulators and Hybrid Systems*. PhD thesis, University of Oslo, 2008.

[15] G.L. Squires. *Practical Physics, Third Edition*. Cambridge University Press, 1985.

[16] Andrew T. Ogielski. Dynamics of three-dimensional ising spin glasses in thermal equilibrium. *Phys. Rev. B*, 32(11):7384–7398, Dec 1985.

[17] Andreas Glatz, Valerii M Vinokur, Joakim Bergli, Martin Kirkengen, and Yuri M Galperin. The coulomb gap and low energy statistics for coulomb glasses. *Journal of Statistical Mechanics: Theory and Experiment*, 2008(06):P06006 (12pp), 2008.

[18] C. Kittel. *Introduction to Solid State Physics*. John Wiley and Sons, Inc, 8 edition, 2005.

[19] J. Kurchan. In and out of equilibrium. *Nature*, 433, 2005.

[20] W. Shockley J. Bardeen. Deformation potentials and mobilities in non-polar crystals. *Physical Review*, 80, 1950.